This article is published as part of the *Dalton Transactions* themed issue entitled:

Dalton Transactions 40th Anniversary

Guest Editor Professor Chris Orvig, Editorial Board Chair
University of British Columbia, Canada

Published in issue 40, 2011 of *Dalton Transactions*

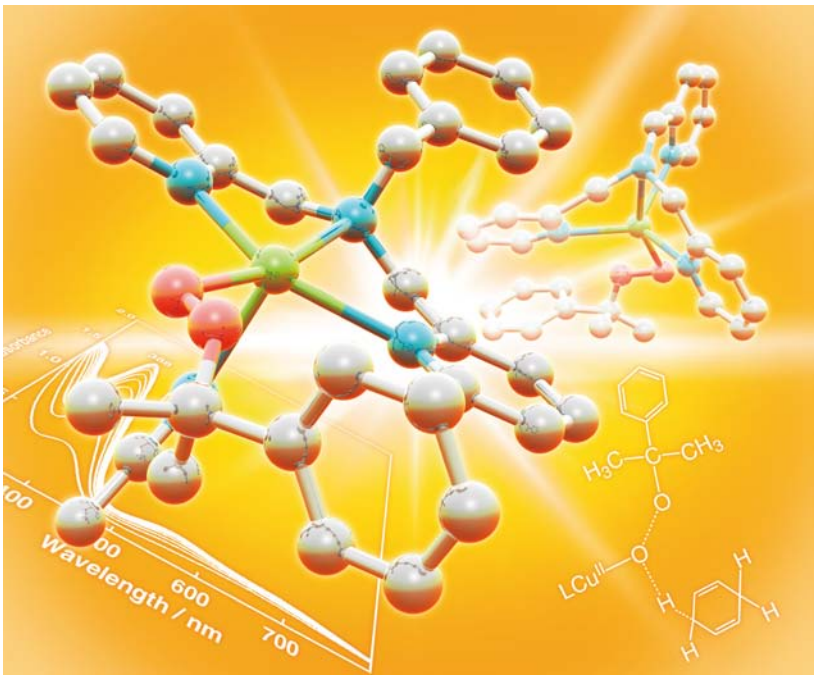

Image reproduced with permission of Shinobu Itoh

Welcome to issue 40 of the 40th volume of Dalton Transactions-40/40! Articles in the issue include:

PERSPECTIVE:

FRONTIER:

ARTICLES:

Visit the *Dalton Transactions* website for more cutting-edge inorganic and organometallic research
www.rsc.org/dalton

Dalton Transactions

Dynamic Article Links

Cite this: *Dalton Trans.*, 2011, **40**, 10416

www.rsc.org/dalton

PAPER

Origins of stereoselectivity in optically pure phenylethaniminopyridine *tris*-chelates $M(NN')_3^{n+}$ (M = Mn, Fe, Co, Ni and Zn)†

Suzanne E. Howson, Laura E. N. Allan, Nikola P. Chmel, Guy J. Clarkson, Robert J. Deeth, Alan D. Faulkner, Daniel H. Simpson and Peter Scott*

Received 6th April 2011, Accepted 24th May 2011
DOI: 10.1039/c1dt10588d

One-pot reactions of 2-pyridinecarboxaldehyde, chiral phenylethanamines and Fe(II) give single diastereomer *fac* diimine complexes at thermodynamic equilibrium so that no chiral separations are required (*d.r.* > 200 : 1). The origins of this stereoselectivity are partly steric and partly a result of the presence of three sets of inter-ligand parallel-offset π-stacking interactions. Mn(II), Co(II), Co(III), Ni(II) and Zn(II) give similar *fac* structures, alongside the imidazole analogues for Fe(II). While most of the complexes are paramagnetic, the series of molecular structures allows us to assess the influence of the π-stacking present, and there is a strong correlation between this and the M–N bond length. Fe(II) is close to optimal. For the larger Zn(II) ion, very weak π-stacking leads to poorer measured stereoselectivity (NMR) but this is improved with increased solvent polarity. The mechanism of stereoselection is further investigated *via* DFT calculations, chiroptical spectroscopy and the use of synthetic probes.

Introduction

The development of methods to synthesise optically pure *tris*-chelate octahedral coordination complexes has been of interest since the beginning of coordination chemistry,[1] but it is a problem still far from solved. Single isomers are required to develop the large number of potential applications in anion recognition,[2,3] molecular sensors,[4,5] supramolecular chemistry,[6,7] DNA targeting,[8,9] protein probes[10] and cancer therapy.[11]

Tris-chelate octahedral complexes with symmetrical (A–A) type ligands, *e.g.* $[Ru(bpy)_3]^{2+}$ are generally formed as racemic mixtures of the Δ and Λ enantiomers (Fig. 1).[1] In some cases with inert metals, *e.g.* Ru(II), these can be resolved by diastereomeric crystallisation with chiral anions[12–15] or by chromatographic techniques, either using a chiral stationary phase[16] or by cation exchange chromatography with chiral anions.[17–19] Determination of the optical purity can, however, be challenging and racemisation is an ever-present issue.[20] For the asymmetric (A–B) ligand class, *e.g.* monosubstituted bipyridines,[21,22] geometric *fac* and *mer* configurations are introduced and, excluding any steric or electronic effects, these are expected in a statistical 1 : 3 ratio. Separation of the four isomers *fac*-Δ, *mer*-Δ, *fac*-Λ and *mer*-Λ, is again only viable for inert complexes and is inherently low-yielding.[23]

Stereoselective syntheses resulting in single isomers are thus a key challenge in this area of coordination chemistry. Current approaches to highly stereoselective syntheses, notably from the Meggers group, involve the use of a temporary chiral auxiliary ligand to favour one enantiomer.[24] The configuration at the metal centre is retained on substitution of the auxiliary for the required ligand in inert complexes only to form *e.g.* enantiomerically pure *tris*-heteroleptic ruthenium(II) complexes with achiral 2,2′-bipyridines.[24,25] Earlier approaches, such as by von Zelewsky, use chiral multidentate ligands to preorganise the configurations at the metal centres forming optically pure octahedral complexes without the need for resolution.[26,27] The syntheses are, however, rather lengthy and the systems are synthetically inflexible.

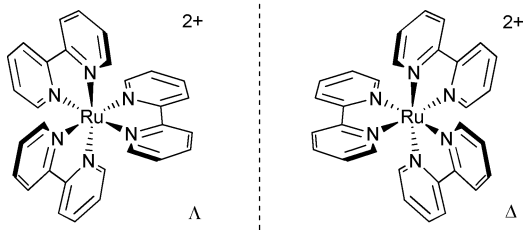

Fig. 1 Enantiomers of $[Ru(bpy)_3]^{2+}$.

An elegant preorganisational technique has been used by the Fletcher[21,28,29] and Weizman[30] groups to allow the exclusive synthesis of *fac* isomers in inert Ru(II) complexes. Tripodal bipyridine ligands force the structures to adopt a *fac* configuration. This method can also control the absolute configuration at the metal through the use of an optically pure chiral tether, resulting in a single diastereomer.[28]

For more labile metals, complete thermodynamic control of the diastereoselection had not been achieved until our recent

Department of Chemistry, University of Warwick, Gibbet Hill Road, Coventry, UK, CV4 7AL. E-mail: peter.scott@warwick.ac.uk; Fax: +44 024 7657 2710; Tel: +44 024 7652 3238

† CCDC reference numbers 821020–821027. For crystallographic data in CIF or other electronic format see DOI: 10.1039/c1dt10588d

report that iron(II) complexes with simple optically pure diimine ligands give optically and stereochemically pure *fac* isomers with *d.r.* > 200 : 1.[31] We describe here an investigation into the origins of this unprecedented stereo- and chemical selectivity in the $[ML_3]^{n+}$ complexes (M = Fe, Co, Ni, Mn, Zn) *via* computational and structural studies, and also the extension to imidazole ligands. We have also recently described the related complexes of achiral hydrazones, which are highly *fac* selective and for which single enantiomers crystallise as conglomerates.[32] We have also commented on some recent related Cu(II) chemistry.[33]

Synthesis of ligand precursors

Optically pure (*R*)-2-phenylglycinol (**4**) was synthesised *via* the reduction of (*R*)-2-phenylglycine using lithium aluminium hydride[34] or, more conveniently on a larger scale (> 15 g), using $NaBH_4/I_2$ *via* an adaptation of a literature procedure.[35] Purification *via* recrystallisation from hot toluene was found to maintain the optical purity of this compound to give an optical rotation value of −25.99° (Lit. = −25.8°).[36] In contrast, distillation was found to result in a partial racemisation leading to a product with an enantiomeric ratio of approximately 7 : 3 (*R*:*S*).

Although protecting group strategies have been used in the synthesis of ether derivatives of 2-phenylglycinol, we found that the direct reaction of the alcohol with halides in the presence of sodium hydride gave the corresponding methyl (**5**)[37] and benzyl (**6**)[38] ethers in good yields.

Imidazole-2-carbaldehydes (**9–11**) were synthesised in high yields from the corresponding *N*-substituted imidazole and dimethylformamide in the presence of *n*-BuLi.[39]

Iron(II) complexes

Following early observations by Busch,[40] three-component 'template' reactions between amine, aldehyde and metal source, rather than simple substitution reactions with pre-formed ligands, are commonly used in the synthesis of complexes of neutral imine ligands. Indeed Burgess and co-workers isolated an 'intermediate' iron(II) species coordinated to two pyridine-imine ligands and one 2-acetylpyridine ligand.[41] We were surprised to find, however, that rather few *tris*-pyridine/imine complexes of Fe(II) have appeared in the literature. We nevertheless used a one-pot strategy, mixing the appropriate amine and 2-pyridinecarboxaldehyde into a solution of $Fe(ClO_4)_2{\cdot}6H_2O$ in acetonitrile (Scheme 1). This led to the immediate formation of intense purple solutions, from which the diamagnetic complexes $[FeL_3][ClO_4]_2$ were isolated.

We found that 4-aminophenol (**1**) gave a product that we could crystallise readily and from the general reaction described above, diamagnetic $[Fe\mathbf{L}^1{}_3][ClO_4]_2$ was isolated in 79% yield. The ^{1}H NMR spectrum of this complex clearly shows the presence of the (racemic) *fac* and *mer* isomers but with a far higher selectivity for *mer* (1 : 15 ratio) than is expected statistically (1 : 3). This gave us our first indication that the stereoselectivity in these complexes could be modified using steric effects. Consequently, we moved to the less bulky benzylamine **2**, which gave diamagnetic $[Fe\mathbf{L}^2{}_3][ClO_4]_2$. The ^{1}H NMR spectrum of this complex indicates a *fac*:*mer* ratio of 1 : 2 [Fig. 2 (a)] - unexpectedly rich in *fac* isomers - and this did not change over time even after prolonged (7 d) heating at 80 °C in air. The exchange between these isomers is

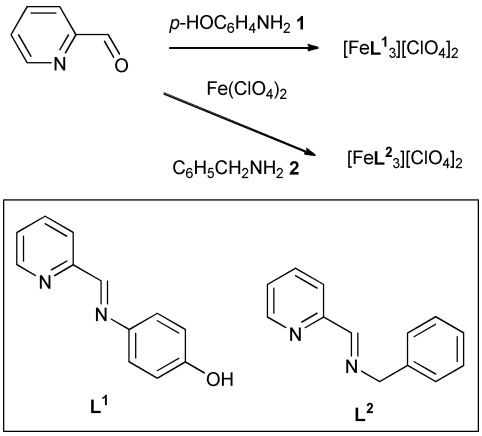

Scheme 1 One-pot syntheses of *tris*-pyridine/imine complexes of Fe(II).

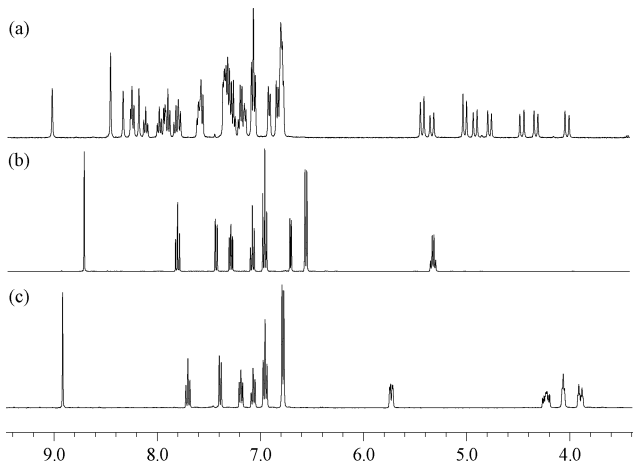

Fig. 2 ^{1}H NMR spectra in CD_3CN of (a) $[Fe\mathbf{L}^2{}_3][ClO_4]_2$, (b) *fac*,$\Lambda_{Fe}$,$R_C$-$[Fe\mathbf{L}^3{}_3][ClO_4]_2$ and (c) *fac*,Δ_{Fe},R_C-$[Fe\mathbf{L}^4{}_3][ClO_4]_2$.

slow on the ^{1}H NMR chemical shift timescale - as expected for a low spin d^6 ion - with distinct resonances observed for the imine units and diastereotopic benzylic CH_2 groups (one set for C_3-symmetric *fac* and three for C_1-symmetric *mer*). We reasoned that this thermodynamic preference for the *fac* isomer could not merely be a steric effect; the bulkier $\mathbf{L}^1$ gave a *mer*-rich system so reducing the steric bulk to $\mathbf{L}^2$ could not in itself encourage the system beyond the statistical ratio of 1 : 3. We were thus encouraged to explore the phenomenon further.

The commercially available (*R*)-α-methylbenzylamine (*e.e.* = 96%) (**3**, Scheme 2) also gave a purple crystalline complex in the standard reaction. Given the long history of this approach described above and also our own explorations of diastereoselection at labile metals[42–47] we were astounded to find that the ^{1}H NMR spectra showed only one set of coordinated ligand signals [Fig. 2 (b)]. The *tris* stoichiometry is confirmed by the diamagnetic nature of the Fe(II) system, microanalysis and mass spectrometric data. Hence a single diastereoisomer with a C_3-symmetric *fac* structure is formed. No further isomers were observed at accessible temperatures or after prolonged storage at elevated temperature, and on the basis that the only impurities present have ^{1}H NMR integrations lower than those of the ^{13}C satellites from the major isomer, the thermodynamic diastereomer ratio must be >200 : 1. By analogy with several molecular structure determinations of

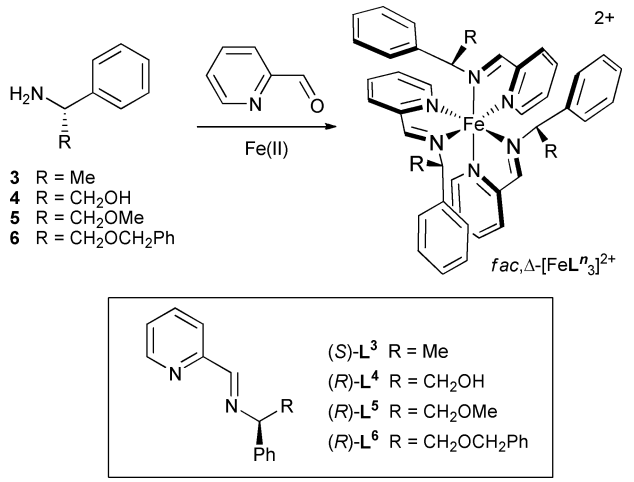

Scheme 2 Single diastereomer complexes $[FeL^{n}_{3}]^{2+}$ (n = **3–8**).

related compounds and following circular dichroism studies (*vide infra*), the structure *fac*,Λ_{Fe},R_C-$[FeL^{3}_{3}][ClO_4]_2$ is assigned (Scheme 2).

The analogous reaction with racemic α-methylbenzylamine (**3**) was investigated using one equivalent each of (*S*)-α-methylbenzylamine and (*R*)-α-methylbenzylamine in the standard procedure. After 24 h the ^{1}H NMR spectrum of the crude product was found to be essentially identical to that of non-racemic *fac*,Λ_{Fe},R_C-$[FeL^{3}_{3}][ClO_4]_2$. Recrystallisation gave a pure sample, which did not alter in diastereomeric composition over time, thus confirming that the thermodynamic product is homochiral.

The use of (*R*)-2-phenylglycinol (**4**) in the standard synthesis led to the isolation of the corresponding highly crystalline trihydroxy complex *fac*,Δ_{Fe},R_C-$[FeL^{4}_{3}][ClO_4]_2$. The ^{1}H NMR spectrum confirmed *d.r.* >200 : 1 as for the L^3 complex [Fig. 2 (c)]. Single crystals were obtained and a single-crystal X-ray structure was determined.

The molecular structure of the cationic unit is shown in Fig. 3, viewed along the approximate C_3 axis, along with key bond lengths and angles. The crystal selected for single-crystal X-ray diffraction had the chiral space group $P2_1$ and allowed the *fac*,Δ_{Fe} geometry to be readily assigned. The asymmetric unit contains two complexes, four perchlorate counterions, an acetonitrile molecule and a water molecule (O23) modelled at half occupancy. The complex is approximately octahedral with an average Fe–N bond length of 1.97 Å, which is close to the expected average (1.958 Å) for this class of low-spin Fe(II) complex.[48] Each of the three pyridine units forms a face-to-face π-stack with a phenyl unit on a neighbouring ligand, with an average angle between the mean planes of the pyridine and phenyl rings of 7.7° and an average centroid–centroid distance of 3.55 Å. These π-stacks contribute to the unprecedented stereoselectivity in this monometallic system (*vide infra*) and orient the CH_2OH groups such that they are mutually directed to encircle the C_3 axis. Each OH group participates in H-bonding with an OH group of another molecular unit, and this is accompanied by short contacts with perchlorate anions and partially-occupied H_2O.

Alongside the issue of stereoselectivity in the *tris*(bidentate) complex $[FeL^{4}_{3}][ClO_4]_2$ it is noteworthy that no *bis*(tridentate) $[FeL^{4}_{2}][ClO_4]_2$ with κ^3-*N*,*N*′,*O* coordinating ligands is detected at equilibrium. This issue is explored later.

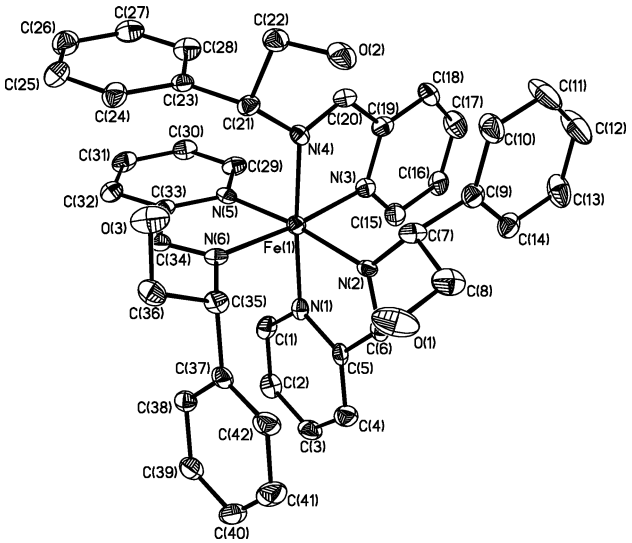

Fig. 3 Structure of one of the independent cations in the asymmetric unit of *fac*,Δ_{Fe},R_C-$[FeL^{4}_{3}][ClO_4]_2\cdot\frac{1}{2}CH_3CN\cdot\frac{1}{4}H_2O$ (H atoms, counterions and solvent molecules omitted for clarity). Thermal ellipsoids are shown at 50% probability. Selected bond lengths (Å) and angles (°): Fe(1)–N(5) 1.967(4), Fe(1)–N(3) 1.969(4), Fe(1)–N(6) 1.970(4), Fe(1)–N(1) 1.970(4), Fe(1)–N(4) 1.983(4), Fe(1)–N(2) 1.991(4), N(2)–C(6) 1.289(7); N(5)–Fe(1)–N(6) 81.23(17), N(3)–Fe(1)–N(4) 81.65(18), N(1)–Fe(1)–N(2) 81.28(16).

The use of the methyl ether[37] **5** in the standard synthesis led to the formation of *fac*,Δ_{Fe},R_C-$[FeL^{5}_{3}][ClO_4]_2$. This complex was also formed as a single diastereomer. The single-crystal X-ray molecular structure (Fig. 4) is analogous to *fac*,Δ_{Fe},R_C-$[FeL^{4}_{3}][ClO_4]_2$.

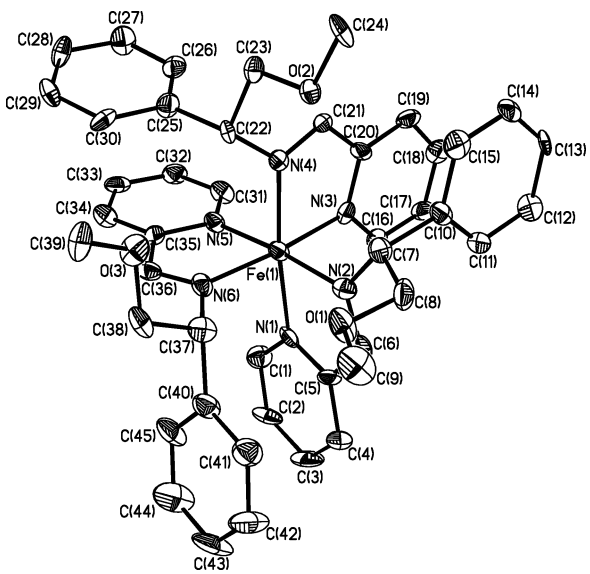

Fig. 4 Structure of the cation in the asymmetric unit of *fac*,Δ_{Fe},R_C-$[FeL^{5}_{3}][ClO_4]_2\cdot 2CH_3CN$ (H atoms, counterions and solvent molecules omitted for clarity). Thermal ellipsoids are shown at 50% probability. Selected bond lengths (Å) and angles (°): Fe(1)–N(6) 1.962(7), Fe(1)–N(3) 1.962(7), Fe(1)–N(5) 1.969(6), Fe(1)–N(2) 1.974(7), Fe(1)–N(1) 1.978(7), Fe(1)–N(4) 1.981(7), N(2)–C(6) 1.264(11); N(5)–Fe(1)–N(6) 81.5(3), N(3)–Fe(1)–N(4) 81.2(3), N(1)–Fe(1)–N(2) 80.5(3).

The use of the benzyl ether[38] **6** in the standard synthesis led to a purple solution as usual but after 2 h at ambient temperature the ^{1}H NMR spectrum of the crude reaction mixture indicated that the kinetic product thus isolated contained one *fac* and one *mer* isomer in an approximate 1 : 1 ratio. This feature is best seen with the four sets of doublet of doublets in the region between 3.60 and 3.20 ppm [Fig. 5 (a)], corresponding to one of the two diastereotopic CHCH_2 protons on the ligands. After heating this sample at 75 °C for 72 h the exclusive (thermodynamic) product *fac*,Δ_{Fe},R_C-[Fe$\mathbf{L}^6{}_3$][ClO_4]$_2$ was formed as for the above complexes [Fig. 5 (b)].

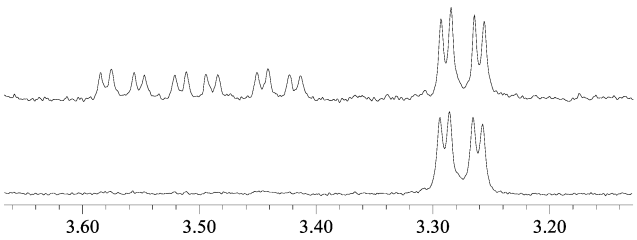

Fig. 5 ^{1}H NMR spectra in CD_3CN of crude samples of R_C-[Fe$\mathbf{L}^6{}_3$][ClO_4]$_2$ after (a) 2 h at ambient temperature and (b) 72 h at 75 °C.

As part of a study into the origins of the stereoselection, we investigated the use of other chiral α-substituted amines. Commercial (*R*)-1-cyclohexylethanamine (*e.e.* = 95%) (**7**) in the standard complex synthesis gave a purple diamagnetic mixture [Fe$\mathbf{L}^7{}_3$][ClO_4]$_2$ containing one *fac* and one *mer* isomer in the thermodynamic ratio 2.6 : 1. While this ratio still strongly favours the *fac* isomer with respect to the statistically expected ratio of 1 : 3, the thermodynamic stereoselectivity is substantially worse than that seen in the analogous *fac*,Λ_{Fe},R_C-[Fe$\mathbf{L}^3{}_3$][ClO_4]$_2$ complex.

Ligand $\mathbf{L}^8$, derived from (*S*)-*tert*-leucinol (**8**), gave in contrast to all the systems above, a paramagnetic crystalline red complex *mer*,S_C-[Fe$\mathbf{L}^8{}_2$][ClO_4]$_2$. The molecular structure as determined by single-crystal X-ray crystallography is shown in Fig. 6. The crystal selected for single-crystal X-ray diffraction had the chiral space group $P2_1$. The asymmetric unit contains the Fe(II) complex with two perchlorate counterions. As well as the nitrogen atoms, the oxygen atoms are also chelated to the iron(II) centre, forming a *bis*(κ^3-*N*,*N*′,*O*) structure. The alcohol hydrogen atoms were located and were found to form short strong H bonds to the perchlorate oxygen atoms with an average distance of 1.97 Å. The average Fe–N bond length is 2.14 Å, close to the expected average (2.13 Å) for this class of high-spin Fe(II) complex.[48] The angle between the mean planes of the two pyridine/imine units is 78.96°. The bond angles between the coordinating atoms making up the distorted octahedron range from 74.25° to 112.61° as a result of the constraints of the chelate. In addition to the single-crystal X-ray studies, microanalysis and NMR studies indicated that the bulk sample comprises this paramagnetic *bis*(κ^3-*N*,*N*′,*O*) complex and no *tris* complex analogous to *fac*,Δ_{Fe},R_C-[Fe$\mathbf{L}^4{}_3$][ClO_4]$_2$ was detected in solution.

Magnetic measurements were conducted in the range 400–2 K for [Fe$\mathbf{L}^8{}_2$][ClO_4]$_2$. The complex remains in the high spin state over the measured temperature range and displays expected paramagnetic behaviour. SQuID magnetometry data led to a μ_{eff} value of 5.30 μ_B at room temperature (298 K), which is as expected for an octahedral high spin Fe(II) complex.[49]

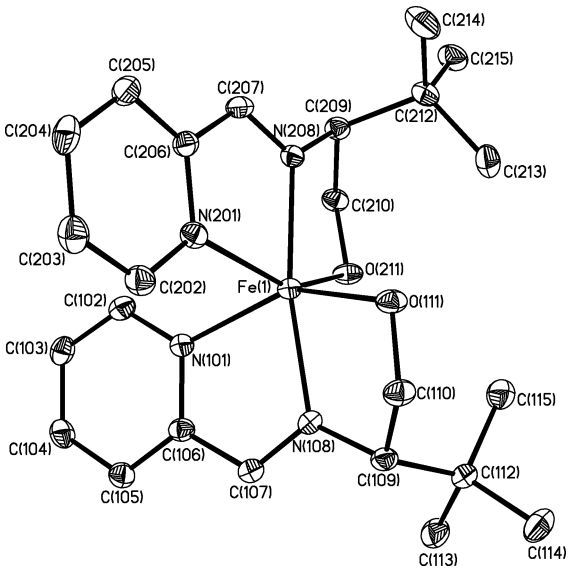

Fig. 6 Structure of the cationic unit in [Fe$\mathbf{L}^8{}_2$][ClO_4]$_2$ (H atoms and counterions omitted for clarity). Thermal ellipsoids are shown at 50% probability. Selected bond lengths (Å) and angles (°): Fe(1)–N(108) 2.1043(17), Fe(1)–O(211) 2.1118(17), Fe(1)–N(208) 2.1178(16), Fe(1)–N(201) 2.1565(19), Fe(1)–O(111) 2.1729(15), Fe(1)–N(101) 2.1952(18), C(107)–N(108) 1.279(3); O(211)–Fe(1)–N(208) 74.36(7), O(211)–Fe(1)–N(201) 147.01(7), N(208)–Fe(1)–N(201) 76.10(7), N(108)–Fe(1)–O(111) 74.25(6), N(108)–Fe(1)–N(101) 76.22(7), O(111)–Fe(1)–N(101) 146.40(6).

We have also investigated the use of 2-imidazole in the place of 2-pyridine in this system (Fig. 7). The one-pot reaction between 1-methyl-1*H*-imidazole-2-carbaldehyde, (*R*)-α-methylbenzylamine and $Fe(ClO_4)_2{\cdot}6H_2O$ in acetonitrile resulted in an intense purple solution. The dropwise addition of ethyl acetate resulted in the precipitation of a dark purple microcrystalline solid. In comparison to the 2-pyridinecarboxaldehyde systems, the resulting complex [Fe$\mathbf{L}^9{}_3$][ClO_4]$_2$ was found to be paramagnetic by ^{1}H NMR spectroscopy. Slow vapour diffusion of ethyl acetate into an acetonitrile solution resulted in single crystals that were suitable for single-crystal X-ray diffraction. The solid state structure of one of the two crystallographically independent but chemically similar iron(II) complexes is shown in Fig. 8.

The crystal has the chiral space group $P2_1$ and the asymmetric unit contains two iron imidazolimine complexes with two partially occupied acetonitrile molecules, in addition to four interspatial perchlorate counterions. The structure shows three ligands arranged around a central iron(II) atom in the *fac*,Λ_{Fe},R_C-[Fe$\mathbf{L}^9{}_3$][ClO_4]$_2$ configuration, in which each of the three *N*-methyl imidazole rings are oriented face-to-face with the phenyl ring of the adjacent ligand. The average angle between the mean planes of these rings (11.8°) is, however, notably larger than those observed in the pyridine Fe(II) structures (*ca* 8°), and the average centroid–centroid bond length of 3.77 Å is substantially longer (*ca* 3.55 Å). Also, unlike the pyridine analogues in which the Fe–N bond lengths are all essentially equivalent, there is a distinct difference between the average Fe–N_{imz} bond length (1.96 Å) and the average Fe–N_{imine} bond length (2.02 Å). This has been observed in related imidazole Schiff base complexes.[50,51]

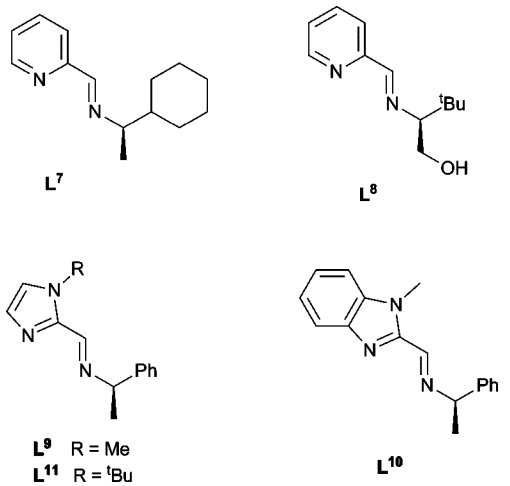

Fig. 7 Ligands $\mathbf{L}^{7}$–$\mathbf{L}^{11}$.

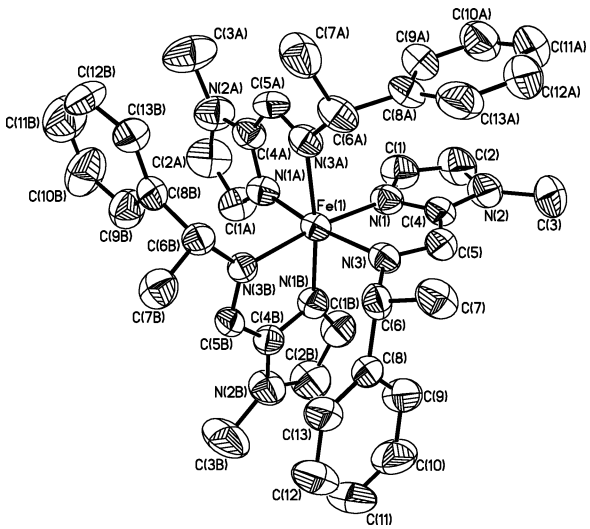

Fig. 8 Structure of one of the independent cations in the asymmetric unit of *fac*,Λ_{Fe},R_C-[Fe$\mathbf{L}^{9}_3$][ClO_4]$_2$·$\frac{1}{2}$$CH_3CN$ (H atoms, counterions and solvent molecules omitted for clarity). Thermal ellipsoids are shown at 50% probability. Selected bond lengths (Å) and angles (°): Fe(1)–N(1A) 1.954(4), Fe(1)–N(1) 1.962(4), Fe(1)–N(1B) 1.963(4), Fe(1)–N(3) 2.011(4), Fe(1)–N(3A) 2.014(4), Fe(1)–N(3B) 2.019(4); N(1)–Fe(1)–N(3) 80.49(16), N(1A)–Fe(1)–N(3A) 81.09(17), N(1B)–Fe(1)–N(3B) 81.00(15).

SQuID measurements on a polycrystalline sample of [Fe$\mathbf{L}^{9}_3$][ClO_4]$_2$ show a gradual increase in magnetic moment from 0.9 to 1.7 μ_B as the temperature increases from 10 to 300 K (Fig. 9). While the magnetic moment for a high spin d^6 complex is expected to fall within the range of 5.0–5.2 μ_B,[49] this reduced value indicates that the complex undergoes partial conversion to high spin over the measured range. The observation of paramagnetic behaviour in the imidazole system is a result of the combined effects of the reduced π donation and π acceptor ability of the ligand.[52–55] Complete spin crossover has previously been reported in analogous *tris*(pyridylbenzimidazole) iron(II) complexes by Boca *et al.*[56] Our own attempt to incorporate a benzimidazole group[57] in this series led to $\mathbf{L}^{10}$, for which we were unable to detect a *tris* complex of Fe(II), presumably for steric reasons. In contrast, the system with an *N*-*tert*-butyl imidazole unit ($\mathbf{L}^{11}$) gave a dark purple paramagnetic solid on complexation with iron(II). Crystals

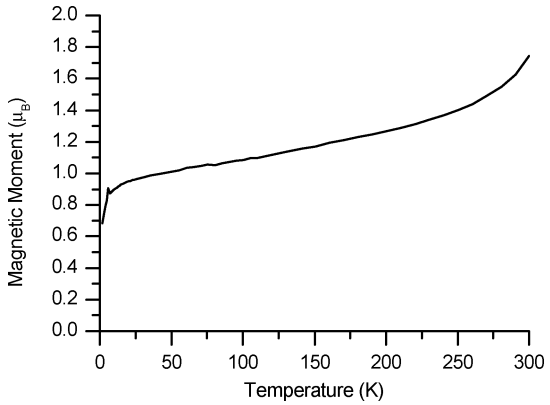

Fig. 9 Plot of magnetic moment *vs.* temperature for [Fe$\mathbf{L}^{9}_3$][ClO_4]$_2$.

suitable for single-crystal X-ray diffraction were obtained through slow vapour diffusion of ethyl acetate into an acetonitrile solution. The resulting molecular structure (Fig. 10) was of the *fac*,Λ_{Fe},R_C-[Fe$\mathbf{L}^{11}_3$][ClO_4]$_2$ diastereomer. The steric hindrance between the phenyl ring and the *N*-*tert*-butyl group results in the complete disruption of the π-stacking observed in the less bulky *N*-methyl analogue. As a result there is a substantial increase in the mean angle between the planes of the phenyl ring and the imidazole to 29.9° and an associated increase in the average centroid–centroid distance (4.22 Å). Inspection of the Fe–N bond lengths again identifies a larger distance for the Fe–N_{imine} bond (1.98 Å) compared to that of the Fe–N_{imz} (1.94 Å). Attempts at assessment of the diastereoselectivity in the bulk sample through powder XRD were hindered by broad and weak diffraction patterns.

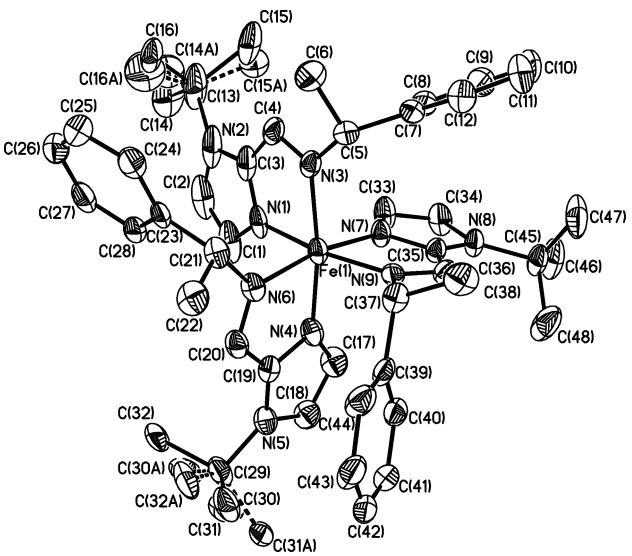

Fig. 10 Structure of the cation in the asymmetric unit of *fac*,Λ_{Fe},R_C-[Fe$\mathbf{L}^{11}_3$][ClO_4]$_2$·1.25CH_3CN (H atoms, counterions and solvent molecules omitted for clarity). Thermal ellipsoids are shown at 50% probability. Selected bond lengths (Å) and angles (°): Fe(1)–N(7) 1.940(3), Fe(1)–N(4) 1.942(3), Fe(1)–N(1) 1.948(3), Fe(1)–N(3) 1.974(3), Fe(1)–N(9) 1.985(3), Fe(1)–N(6) 1.989(3); N(1)–Fe(1)–N(3) 81.14(15), N(4)–Fe(1)–N(6) 80.73(12), N(7)–Fe(1)–N(9) 80.47(12).

Zinc(II) complexes

Colourless complexes of Zn(II) with $\mathbf{L}^3$ and $\mathbf{L}^4$ were readily isolated *via* the use of zinc(II) tetrafluoroborate hydrate. In the case of R_C-$\mathbf{L}^3$, the molecular structure (Fig. 11) of the compound is the *fac*,Λ_{Zn},R_C-[Zn$\mathbf{L}^3{}_3$][ClO_4]$_2$ isomer as expected on the basis of the above Fe(II) chemistry *i.e.* the structure recorded is the mirror image of *fac*,Δ_{Fe},R_C-[Fe$\mathbf{L}^4{}_3$][ClO_4]$_2$.

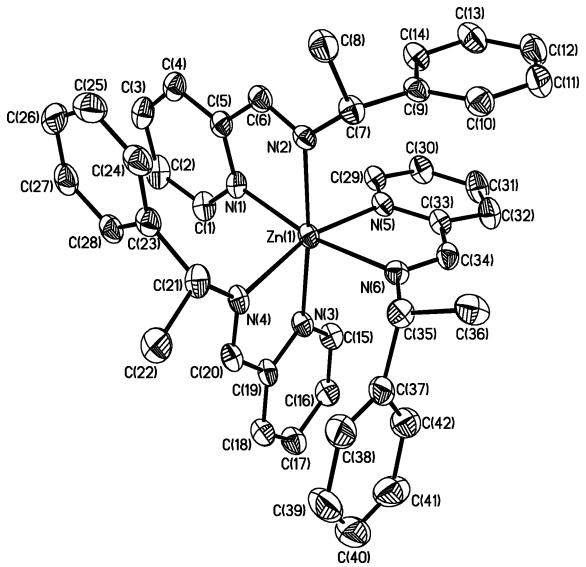

Fig. 11 Structure of the cationic unit in *fac*,Λ_{Zn},R_C-[Zn$\mathbf{L}^3{}_3$][ClO_4]$_2$·CH_3CN·EtOAc (H atoms, counterions and solvent omitted for clarity). Thermal ellipsoids are shown at 50% probability. Selected bond lengths (Å) and angles (°): Zn(1)–N(1) 2.155(2), Zn(1)–N(5) 2.157(2), Zn(1)–N(2) 2.158(2), Zn(1)–N(3) 2.175(2), Zn(1)–N(6) 2.189(2), Zn(1)–N(4) 2.199(2), N(2)–C(6) 1.268(4); N(1)–Zn(1)–N(2) 77.32(10), N(3)–Zn(1)–N(4) 77.11(9), N(5)–Zn(1)–N(6) 76.82(10).

In solution, the ^{1}H NMR spectrum of R_C-[Zn$\mathbf{L}^3{}_3$][BF_4]$_2$ at 298 K revealed the presence of two isomers, which on the basis of the 3-fold symmetry of one isomer and computations (*vide infra*) are assigned as *fac*,Λ_{Zn} (major) and *mer*,Λ_{Zn} (minor). This poorer stereoselectivity gives us the opportunity to probe the effect of solvent polarity on the diastereomeric ratio using ^{1}H NMR spectroscopy. The complex is not soluble in protic media such as methanol but it is conveniently soluble in various mixtures of acetonitrile (polarity index 5.8) and dichloromethane (polarity index 3.1). Fig. 12 shows that the *fac*/*mer* ratio increases with solvent polarity. This is discussed further in relation to comparisons of crystallographic data.

With the potentially tridentate $\mathbf{L}^4$, Zn(II) gave a complex mixture of products, probably comprising various diastereomers of *tris* and *bis* ligand species. However, in the crystallised solid microanalysis was consistent with the presence of predominantly the *bis* ligand complex [Zn$\mathbf{L}^4{}_2$][BF_4]$_2$, analogous to [Fe$\mathbf{L}^8{}_2$][ClO_4]$_2$. Hence it appears that with Zn(II), where κ^3 coordination of the ligand is possible, for example with $\mathbf{L}^3$ (κ^3-*N*,*N*′,*O*), a non-chemoselective reaction is present.

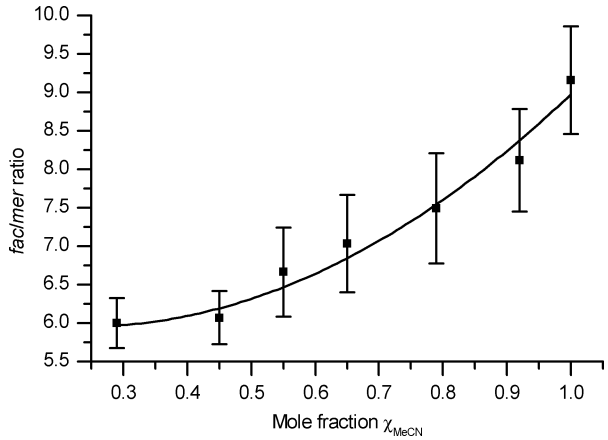

Fig. 12 Change in the *fac*/*mer* ratio of Λ_{Zn},R_C-[Zn$\mathbf{L}^3{}_3$][BF_4]$_2$ with solvent polarity.

Cobalt(II) complex

The addition of cobalt(II) chloride to a methanol solution containing pre-formed $\mathbf{L}^3$ led to the immediate formation of a bright orange solution. Analytically pure crystals of the paramagnetic complex [Co$\mathbf{L}^3{}_3$][PF_6]$_2$ were readily isolated following addition of sodium hexafluorophosphate. Crystals suitable for single-crystal X-ray crystallography were grown from the methanol filtrate. The molecular structure of this compound is shown in Fig. 13 and is the *fac*,Λ_{Co},R_C-[Co$\mathbf{L}^3{}_3$][PF_6]$_2$ isomer, as expected from the Fe(II) chemistry. The structure is analogous to the mirror image of *fac*,Δ_{Fe},R_C-[Fe$\mathbf{L}^4{}_3$][ClO_4]$_2$.

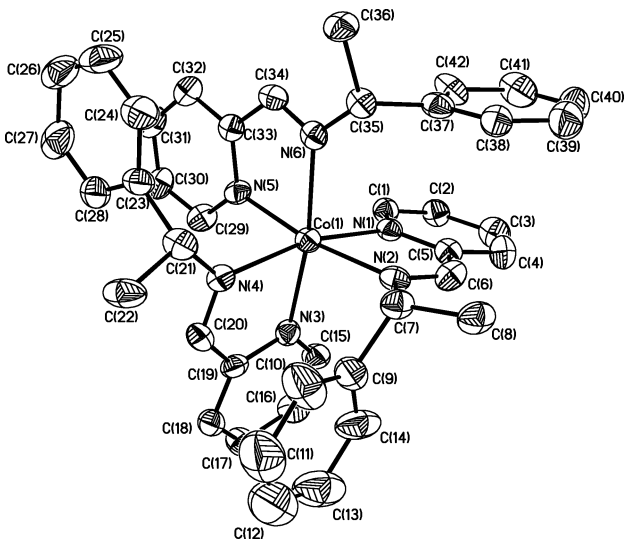

Fig. 13 Structure of the cationic unit in *fac*,Λ_{Co},R_C-[Co$\mathbf{L}^3{}_3$][PF_6]$_2$·2MeOH (H atoms, counterions and solvent omitted for clarity). Thermal ellipsoids are shown at 50% probability. Selected bond lengths (Å) and angles (°): Co(1)–N(1) 2.125(4), Co(1)–N(3) 2.139(4), Co(1)–N(2) 2.152(4), Co(1)–N(6) 2.152(4), Co(1)–N(4) 2.163(4), Co(1)–N(5) 2.167(4), N(2)–C(6) 1.259(6); N(1)–Co(1)–N(2) 77.61(15), N(3)–Co(1)–N(4) 77.66(15), N(5)–Co(1)–N(6) 77.20(15).

Magnetic measurements were conducted in the range 340–2 K for [Co$\mathbf{L}^3{}_3$][PF_6]$_2$. The complex remains in the high spin state over this range and displays expected paramagnetic behaviour. The

SQuID magnetometry data leads to a μ_{eff} value of 4.86 μ_B at room temperature; values between 4.7 and 5.2 μ_B are typically observed for octahedral high spin Co(II) complexes.[49] Evans' NMR method gave the same value in solution.

Cobalt(III) complex

Rather few *tris*-diimine complexes of Co(III) are known, presumably because in this ligand environment the Co(II) state is expected to be stabilised. The synthesis of this compound from cobalt(II) precursors *via* oxidation was unsuccessful. Use of an oxidising agent, *e.g.* H_2O_2 or Cp_2FePF_6, resulted in a mixture of cobalt(III) and cobalt(II) compounds. Finally, the reaction between the proligand and the cobalt(III) precursor $Na_3[Co(NO_2)_6]$ gave the desired complex, $[Co\mathbf{L}^3{}_3][PF_6]_3$. This complex was found to be unstable and decomposed rapidly, thus preventing detailed analysis on a pure sample. The major species in the ^{1}H NMR spectrum of $[Co\mathbf{L}^3{}_3][PF_6]_3$ appears to be the *fac* isomer and while other minor components were observed, the instability of the system means that we are unable to exclude the strong possibility that these are *e.g.* diamagnetic solvated *bis* complexes. The stereoselectivity in this product is thus unknown.

A molecular structure of the cobalt(III) complex has nevertheless been obtained (Fig. 14), and reveals that the isomer was *fac*,Δ_{Co},S_C-$[Co\mathbf{L}^3{}_3][PF_6]_3$, as expected from the Fe(II) system. The single-crystal X-ray molecular structure is analogous to *fac*,Δ_{Fe},R_C-$[Fe\mathbf{L}^4{}_3][ClO_4]_2$.

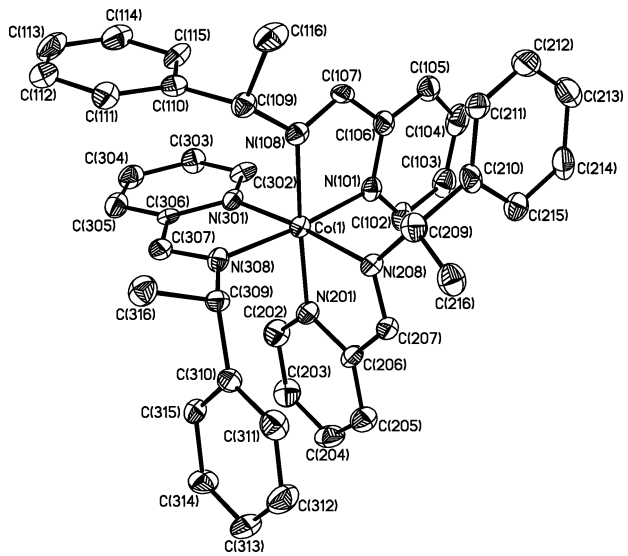

Fig. 14 Structure of the cationic unit in *fac*,Δ_{Co},S_C-$[Co\mathbf{L}^3{}_3][PF_6]_3$·$3CH_3CN$ (H atoms, counterions and solvent omitted for clarity). Thermal ellipsoids are shown at 50% probability. Selected bond lengths (Å) and angles (°): Co(1)–N(201) 1.932(4), Co(1)–N(101) 1.934(4), Co(1)–N(308) 1.937(4), Co(1)–N(301) 1.939(4), Co(1)–N(108) 1.959(4), Co(1)–N(208) 1.962(4), N(108)–C(107) 1.285(7); N(101)–Co(1)–N(108) 83.73(19), N(201)–Co(1)–N(208) 83.21(17), N(301)–Co(1)–N(308) 83.53(18).

Nickel(II) complex

A light red-brown coloured paramagnetic complex of Ni(II) with $\mathbf{L}^3$ was readily isolated in a good yield *via* the use of nickel(II) perchlorate hexahydrate. The molecular structure (Fig. 15) of this compound is the *fac*,Δ_{Ni},S_C-$[Ni\mathbf{L}^3{}_3][ClO_4]_2$ isomer as expected on the basis of the above Fe(II) chemistry *i.e.* the structure recorded is analogous to *fac*,Δ_{Fe},R_C-$[Fe\mathbf{L}^4{}_3][ClO_4]_2$.

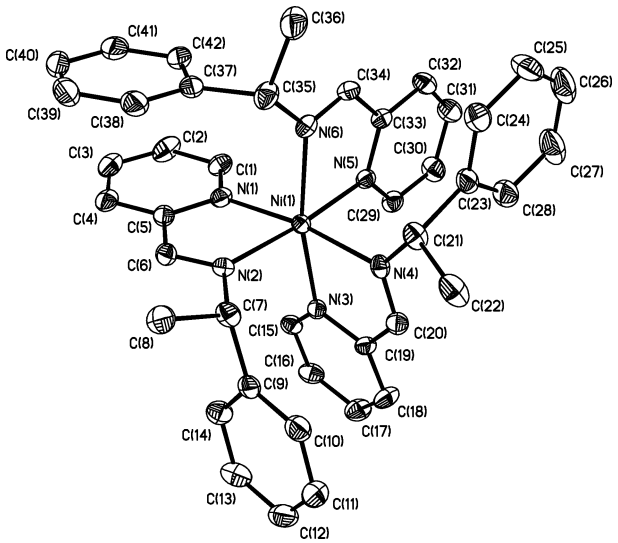

Fig. 15 Structure of the cationic unit in *fac*,Δ_{Ni},S_C-$[Ni\mathbf{L}^3{}_3][ClO_4]_2$·$CH_3CN$·EtOAc (H atoms, counterions and solvent omitted for clarity). Thermal ellipsoids are shown at 50% probability. Selected bond lengths (Å) and angles (°): Ni(1)–N(3) 2.082(3), Ni(1)–N(5) 2.094(3), Ni(1)–N(1) 2.097(3), Ni(1)–N(2) 2.102(3), Ni(1)–N(4) 2.117(3), Ni(1)–N(6) 2.138(3), C(6)–N(2) 1.275(4); N(1)–Ni(1)–N(2) 78.97(11), N(3)–Ni(1)–N(4) 79.06(10), N(5)–Ni(1)–N(6) 79.12(10).

Manganese(II) complex

The use of manganese(II) perchlorate hexahydrate with $\mathbf{L}^3$ in the standard procedure resulted in the formation of a yellow Mn(II) complex. The molecular structure (Fig. 16) of this compound is

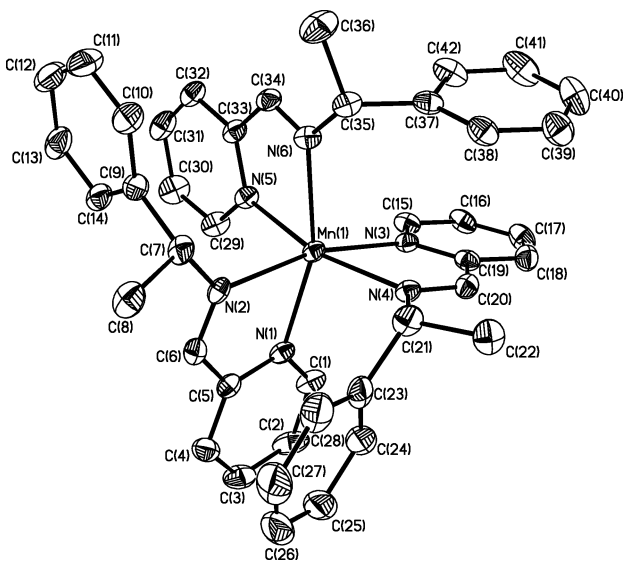

Fig. 16 Structure of the cationic unit in *fac*,Λ_{Mn},R_C-$[Mn\mathbf{L}^3{}_3][ClO_4]_2$·$2CH_3CN$ (H atoms, counterions and solvent omitted for clarity). Thermal ellipsoids are shown at 50% probability. Selected bond lengths (Å) and angles (°): Mn(1)–N(6) 2.240(2), Mn(1)–N(3) 2.254(2), Mn(1)–N(1) 2.258(3), Mn(1)–N(2) 2.273(2), Mn(1)–N(5) 2.284(3), Mn(1)–N(4) 2.285(2), C(6)–N(2) 1.276(4); N(1)–Mn(1)–N(2) 73.91(9), N(3)–Mn(1)–N(4) 73.98(9), N(5)–Mn(1)–N(6) 73.59(9).

the *fac*,Λ_{Mn},R_C-[Mn$\mathbf{L}^3{}_3$][ClO_4]$_2$ isomer as expected from the Fe(II) system, *i.e.* the Mn(II) structure is the mirror image of *fac*,Δ_{Fe},R_C-[Fe$\mathbf{L}^4{}_3$][ClO_4]$_2$.

Spectroscopy

UV-vis absorbance spectra for the Fe(II), Zn(II), Co(II), Ni(II) and Mn(II) complexes with ligand $\mathbf{L}^3$, and the iron(II) imidazolimine complex R_C-[Fe$\mathbf{L}^9{}_3$][ClO_4]$_2$ in acetonitrile are shown in Fig. 17.

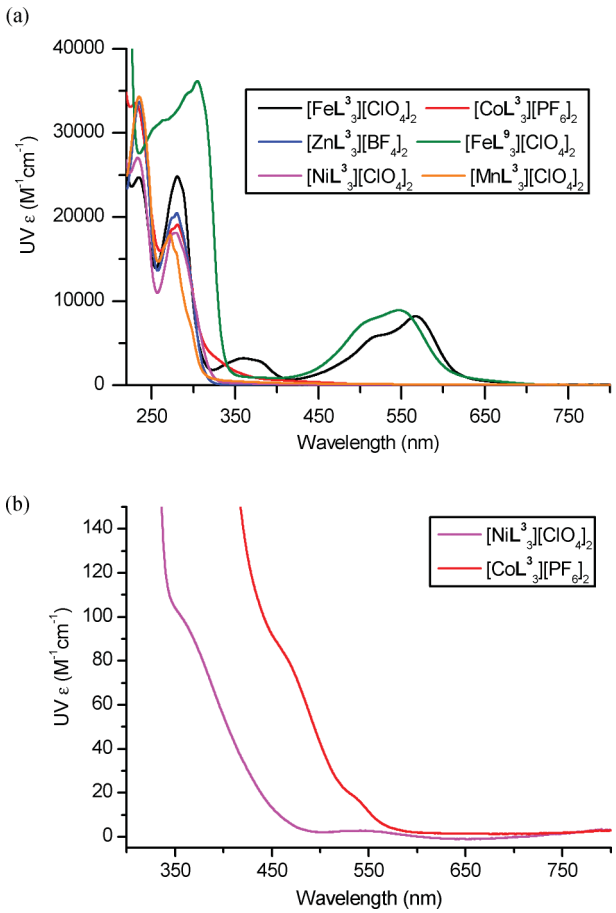

Fig. 17 UV-vis absorbance spectra of *fac*,Λ_{Fe},R_C-[Fe$\mathbf{L}^3{}_3$][ClO_4]$_2$, R_C-[Co$\mathbf{L}^3{}_3$][PF_6]$_2$, Λ_{Zn},R_C-[Zn$\mathbf{L}^3{}_3$][BF_4]$_2$, S_C-[Ni$\mathbf{L}^3{}_3$][ClO_4]$_2$, R_C-[Mn$\mathbf{L}^3{}_3$][PF_6]$_2$ and R_C-[Fe$\mathbf{L}^9{}_3$][ClO_4]$_2$ in acetonitrile. The path length was 1.0 cm and the concentration was (a) 0.03 mM and (b) 1.0 mM showing shoulders in Ni and Co spectra corresponding to *d-d* and/or MLCT transitions.

All complexes have strong bands in the region 220–320 nm, corresponding to π–π* transitions in the ligands. The UV-vis spectrum of *fac*,Λ_{Fe},R_C-[Fe$\mathbf{L}^3{}_3$][ClO_4]$_2$ has strong MLCT transition bands between 320 and 700 nm. The main MLCT band has two distinct maxima at *ca* 567 nm (ε = 8100 M^{-1} cm^{-1}) and 520 nm (ε = 5800 M^{-1} cm^{-1}). The slight structural deviation from a perfect octahedron gives rise to an additional third MLCT band at *ca* 360 nm (ε = 3200 M^{-1} cm^{-1}). The bands are at comparable wavelengths and relative intensities to the corresponding peaks assigned to MLCT transitions in the CD spectrum (*vide infra*).

The UV-vis spectrum of R_C-[Fe$\mathbf{L}^9{}_3$][ClO_4]$_2$ has overlapping bands in the region 250–350 nm, associated with π–π* transitions.[50] The MLCT region has two distinct maxima at *ca* 547 nm (ε = 9000 M^{-1} cm^{-1}) and 504 nm (ε = 7300 M^{-1} cm^{-1}).

The spectrum of the cobalt(II) complex contains a very broad signal corresponding to MLCT transitions at *ca* 340 nm (ε = 2300 M^{-1} cm^{-1}), which appears as a shoulder on the π–π* bands at *ca* 280 nm. This MLCT signal is significantly less intense than these transitions in the iron(II) analogue, which consistent with the notably less intense colour of the crystals and solutions of R_C-[Co$\mathbf{L}^3{}_3$][PF_6]$_2$ compared with *fac*,Λ_{Fe},R_C-[Fe$\mathbf{L}^3{}_3$][ClO_4]$_2$. The lower intensity and the shift to a higher frequency is consistent with the poorer π-donor character of cobalt(II).[58] At higher concentration (1.0 mM), two further signals can be detected at *ca* 465 nm (ε = 80 M^{-1} cm^{-1}) and 535 nm (ε = 20 M^{-1} cm^{-1}) corresponding to Laporte-forbidden but spin-allowed *d-d* transitions.

The spectrum of the manganese(II) complex also has a shoulder on the π–π* bands corresponding to the MLCT transitions. As expected, no *d-d* transitions are observed for this complex as they are both Laporte and spin forbidden.

The spectrum of the nickel(II) complex has no MLCT bands as expected. At higher concentration (1.0 mM), two signals can be detected at *ca* 360 nm (ε = 100 M^{-1} cm^{-1}) and 545 nm (ε = 3 M^{-1} cm^{-1}) corresponding to Laporte-forbidden but spin-allowed *d-d* transitions.

The spectrum of the zinc(II) complex is comparably less interesting than the spectra of the other metal complexes. The absence of any bands above 320 nm is consistent with no MLCT or *d-d* transitions as expected for a d^{10} octahedral complex.

The circular dichroism (CD) spectra for the Fe(II), Zn(II), Co(II), Ni(II) and Mn(II) complexes with ligand $\mathbf{L}^3$, and the iron(II) imidazolimine complex R_C-[Fe$\mathbf{L}^9{}_3$][ClO_4]$_2$ in acetonitrile are shown in Fig. 18. The spectrum of the opposite enantiomer for the iron(II) complex, *fac*,Δ_{Fe},S_C-[Fe$\mathbf{L}^3{}_3$][ClO_4]$_2$ was also collected for comparison. All peaks are at comparable wavelengths and relative intensities to the corresponding bands in the UV-vis absorbance spectra (*vide supra*).

The CD spectra of the iron(II) complexes with $\mathbf{L}^3$, *fac*,Λ_{Fe},R_C- and *fac*,Δ_{Fe},S_C-[Fe$\mathbf{L}^3{}_3$][ClO_4]$_2$, contain intense features spanning the whole UV-vis region and are equal and opposite for the enantiomeric pair. The intense bisignate curves centred around 574 nm result from strong exciton coupling in the MLCT transitions (as well as small contributions from Laporte-forbidden *d-d* transitions) and confirm the formation of non-racemic chiral metal centres.[59,60] The third MLCT band is observed around 360 nm.[59,60] These MLCT bands are also visible in the UV-vis spectrum as three peaks (*vide supra*). All bands at lower wavelengths in the CD spectrum (220–335 nm) result from π–π* transitions within the ligands. Comparison of the CD spectra of the structurally similar Δ and Λ $[Fe(bpy)_3]^{2+}$ enantiomers confirms the electronic transition assignments and the configuration assignments, Δ_{Fe} for S_C-$\mathbf{L}^3$ and Λ_{Fe} for R_C-$\mathbf{L}^3$.[60,61]

The CD spectrum of the R_C-[Fe$\mathbf{L}^9{}_3$][ClO_4]$_2$ complex also contains intense features spanning the whole UV-vis region, with an intense bisignate curve centred around 553 nm consistent with the predominance of the expected Λ_{Fe} isomer in solution.

The CD spectra of R_C-[Co$\mathbf{L}^3{}_3$][PF_6]$_2$, Λ_{Zn},R_C-[Zn$\mathbf{L}^3{}_3$][BF_4]$_2$, R_C-[Mn$\mathbf{L}^3{}_3$][BF_4]$_2$ and S_C-[Ni$\mathbf{L}^3{}_3$][BF_4]$_2$ also have bands in the

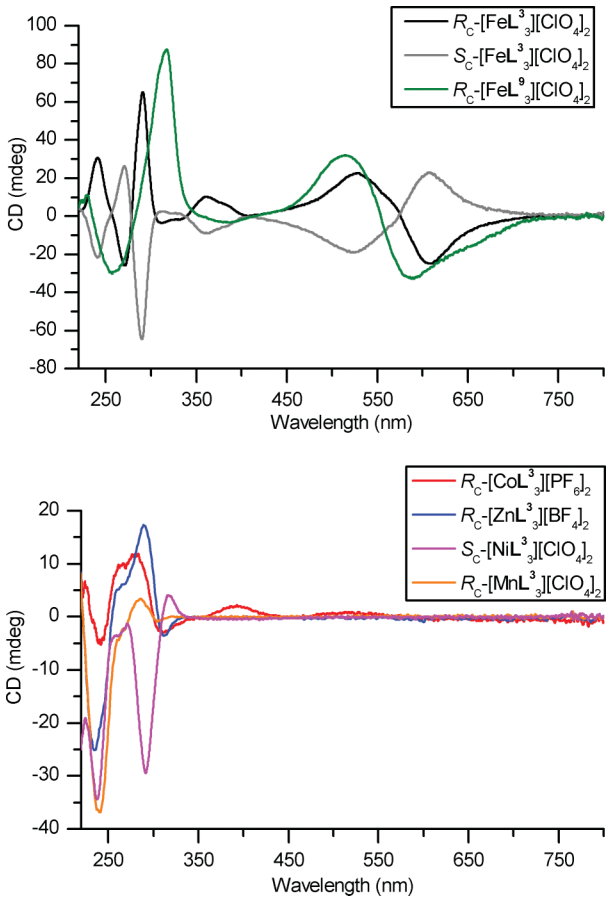

Fig. 18 CD spectra of *fac*,Λ_{Fe},R_C-[FeL$^3_3$][ClO$_4$]$_2$, R_C-[CoL$^3_3$][PF$_6$]$_2$, Λ_{Zn},R_C-[ZnL$^3_3$][BF$_4$]$_2$, S_C-[NiL$^3_3$][ClO$_4$]$_2$, R_C-[MnL$^3_3$][PF$_6$]$_2$ and R_C-[FeL$^9_3$][ClO$_4$]$_2$ in acetonitrile. The concentration was 0.03 mM and the path length was 1.0 cm.

lower wavelength region (220–335 nm) as expected from π–π* transitions within the chiral ligands. In addition, the spectrum of R_C-[CoL$^3_3$][PF$_6$]$_2$ also contains weak bands at *ca* 395 nm and 520 nm corresponding to weak MLCT and *d*-*d* transitions.[58] This confirms the presence of non-racemic chiral metal centres in solution for this paramagnetic compound, although this cannot be taken as a measure of stereoselectivity.[33] The absence of any observable MLCT bands in the zinc(II), nickel(II) and manganese(II) complexes does not allow for any conclusions to be made about the chirality at these metal centres.

Origins of stereo- and chemical selectivity

It is evident that for the above complex cations [FeL$''_3$]$^{2+}$ (n = 3–6) the product contains only one of four possible κ^2-*N*,*N*′ diastereomers *i.e.* there is essentially perfect thermodynamic stereoselection with respect to the absolute configuration at the metal.

For the **L**^{7} complex the *fac*:*mer* ratio was found to be 2.6 : 1. Although cyclohexyl is rather larger than phenyl and is not capable of π-stacking, the isomeric ratio still substantially favours the *fac* configuration. Hence, steric factors also appear to promote the formation of the observed major isomer.

For the bulkier **L**^{8}, an analysis of a simple molecular mechanics model indicates that the *tris* structure is sterically untenable, *i.e.* *tert*-butyl is too large a group to be accommodated. Consequently the less crowded *bis*(tridentate) structure is favoured. Clearly also the presence of a third ligating atom promotes this structure as a result of the chelate effect, and arguably the greater surprise is the formation of *tris*(bidentate) *fac*,Δ_{Fe},R_C-[FeL$^4_3$][ClO$_4$]$_2$ described above.

The single crystal X-ray crystallographic studies above show that the observed *fac* diastereomers display three concurrent π-stacks. The mutual arrangement of the rings is close to what is regarded as optimum within this parallel-displaced regime (as opposed to CH-π) *i.e.* the rings are laterally displaced with the C atom of one ring over the centroid of the other.[62] The key structural parameters determined for all the above complexes are summarised in Table 1, focusing on the various parameters associated with these π-stacks (Fig. 19).

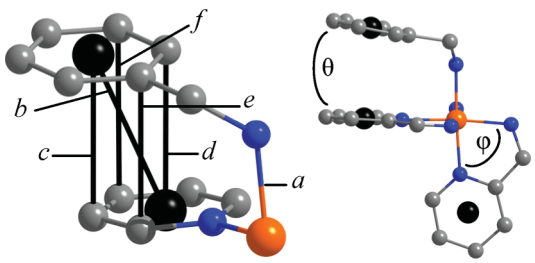

Fig. 19 Defining the π-stacking parameters in Table 1. Distances a = average M–N, b = arene centroid–centroid, c = carbon (Py) to centroid (Ph), d = carbon (Ph) to centroid (Py), e = between substituted carbon atoms, f = between carbon atoms *meta* to substituted carbon atoms; angles θ = between ring planes, φ = average chelate bite.

Table 1 Selected structural parameters for the iminopyridine complexes *fac*-[ML$''_3$]$^{n+}$ [M = Fe(II), Co(III), Ni(II), Co(II), Zn(II) and Mn(II)]

	Fe(II)		Co(III)	Ni(II)	Co(II)	Zn(II)	Mn(II)
Parameter	**L**^{4}	**L**^{5}	**L**^{3}				
a/Å	1.98	1.97	1.94	2.10	2.15	2.17	2.27
b/Å	3.48–3.64	3.51–3.63	3.49–3.73	3.64–4.00	3.75–4.45	3.67–4.08	4.09–4.26
c/Å	3.28–3.50	3.29–3.47	3.27–3.53	3.45–3.72	3.54–4.22	3.50–3.83	3.82–4.05
d/Å	3.24–3.45	3.28–3.43	3.26–3.35	3.26–3.57	3.35–3.70	3.30–3.61	3.54–3.98
e/Å	3.15–3.25	3.19–3.23	3.14–3.21	3.38–3.46	3.48–3.75	3.47–3.55	3.66–3.84
f/Å	3.36–3.71	3.40–3.65	3.49–3.62	3.30–3.91	3.43–4.27	3.33–3.97	3.71–4.27
θ/°	5.41–11.14	5.03–11.21	9.73–12.30	5.83–13.98	3.78–11.21	3.58–14.12	6.37–15.13
φ/°	81.36	81.10	83.49	79.05	77.49	77.08	73.83

For the Fe(II) and Co(III) structures with relatively short M–N distances (*a*), the relevant arene centroid-centroid distances (*b*) are in the range 3.48–3.73 Å, close to the calculated optimum distance of 3.5 Å.[62] The relevant C–centroid distances (*c* and *d*) are in the range 3.24–3.53 Å, the inter-ring distances between the substituted C atoms (*e*) are structurally constrained to be at rather short distances of 3.14–3.25 Å, while the contacts *meta* to these (*f*) are found in the range 3.36–3.71 Å. Fig. 20 shows the favourable arrangement of the π-stacked rings in one of the Fe(II) complexes (the Co(III) structure is similar). The nature and energy of such non-covalent bonding interactions is an area of intense study and debate,[63] not least because of their significant contribution to the stability of important supramolecular structures such as DNA and proteins. Calculations analysed at the SCS-MP2/aug-cc-pVTZ level of theory by Hohenstein and Sherrill allow us to estimate that each contact in our system contributes *ca* 3 kcal mol^{-1}.[62]

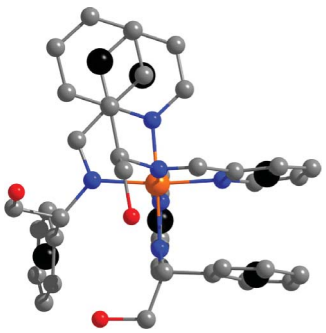

Fig. 20 Molecular structure of *fac*,Δ_{Fe},R_C-[Fe$\mathbf{L}^4_3$]$^{2+}$ showing the offset π-stacking. The view is with the relevant phenyl ring uppermost and in the plane of the page. Ring centroids are shown as black spheres.

In comparison to the Fe(II)/Co(III) complexes, the average M–N distances (*a*) in the Ni(II), Co(II), Zn(II) and Mn(II) complexes are substantially longer and increase in that order (Table 1), resulting in smaller chelate bite angles (φ). The presence of these longer M–N bonds moves the benzylic phenyl group away from the adjacent pyridine ring so that the π-stacking interaction is reduced, as can be seen in the centroid–centroid distances (*b*) and the two centroid–C atom distances (*c* and *d*). The rather short C–C distances (*e*) (*ca.* 3.2 Å) in the Fe(II)/Co(III) complexes resulting from the structural constraints mentioned earlier are relaxed to 3.4–3.8 Å for the other metals studied, and this is accompanied by angles between the planes for the π-stacks (θ) as low as 3.6 Å for Zn(II). Of all these parameters, however, we feel that the centroid–centroid distance (*b*) gives the readiest assessment of the interaction since all the other distances and angles have an impact on it.

Fig. 21 shows that for the Co(II) complex there is essentially no π-stacking, and the situation is similar for the larger metals Zn(II) and Mn(II). This corresponds with our observation of poorer stereoselectivity for Zn(II) than Fe(II). Most interesting, however, is our observation *via* NMR spectroscopy previously (Fig. 12) that increasing polarity improves the stereoselectivity in the Zn(II) system. This is presumably because the hydrophobic π-stacking is promoted, although we cannot exclude effects arising from a difference in the overall polarity of the two isomers.

The relative energies of the relevant diastereomers of S_C-[Fe$\mathbf{L}^3_3$]$^{2+}$ were investigated by computational means. The four different possible (low spin) geometries were optimised and their

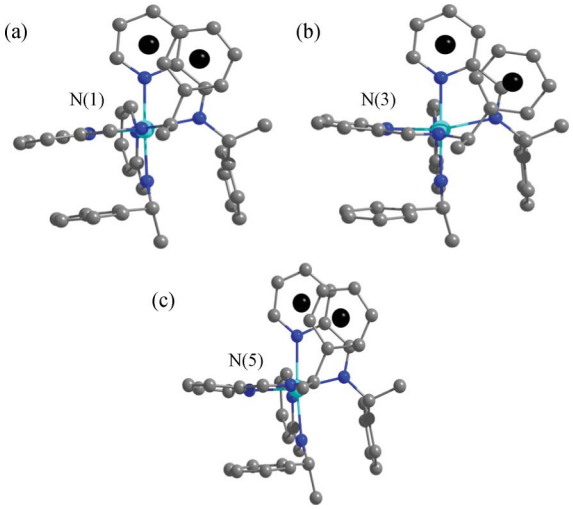

Fig. 21 The molecular structure of *fac*,Λ_{Co},R_C-[Co$\mathbf{L}^3_3$]$^{2+}$ showing the π-stacking. In all cases the view is with the relevant phenyl ring uppermost and in the plane of the page. Ring centroids are shown as black spheres.

energies calculated from density functional calculations using ADF 2008 (version 2008.01; see experimental section).[64] The optimised structures are shown in Fig. 22.

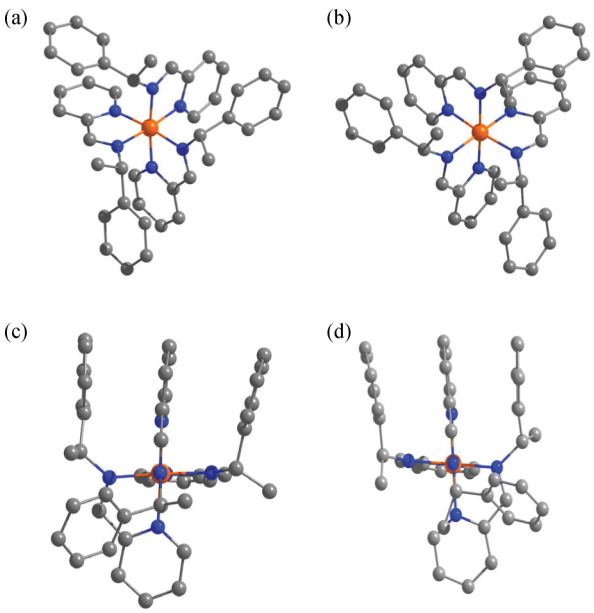

Fig. 22 Optimised dicationic structures of (a) *fac*,Δ_{Fe},S_C-[Fe$\mathbf{L}^3_3$]$^{2+}$, (b) *fac*,Λ_{Fe},S_C-[Fe$\mathbf{L}^3_3$]$^{2+}$, (c) *mer*,Δ_{Fe},S_C-[Fe$\mathbf{L}^3_3$]$^{2+}$, (d) *mer*,Λ_{Fe},S_C-[Fe$\mathbf{L}^3_3$]$^{2+}$.

The observed isomer *fac*,Δ_{Fe} [Fig. 22 (a)] is essentially superimposable on the appropriate subunit of the molecular structure of *fac*,Δ_{Fe},R_C-[Fe$\mathbf{L}^4_3$]$^{2+}$. As expected, this isomer has the lowest energy, followed by the *mer*,Δ_{Fe} isomer [Fig. 22 (c)] *ca* 10 kcal mol^{-1} higher. This is consistent with the observation by NMR spectroscopy of a minor *mer* isomer in the R_C-[Zn$\mathbf{L}^3_3$][BF_4]$_2$ system. The optimised *mer*,Δ_{Fe} structure reveals extended π-stacking involving each of the three ligands; a pyridine ring from one ligand with phenyl rings either side, with each ring aligning

approximately parallel to the next [Fig. 22 (c)].‡ While we are not aware of computed figures for the energy of such an extended π-stacked system we estimate that it would provide substantially less stabilisation to the structure than three offset parallel π-stacked rings in the lower energy *fac*,Δ_{Fe} structure.

The two optimised Λ_{Fe} structures - *fac*,Λ_{Fe} [Fig. 22 (b)] and *mer*,Λ_{Fe} [Fig. 22 (d)] - have similar energies, higher than *fac*,Δ_{Fe} by *ca* 25 kcal mol^{-1}. Interestingly the *fac*,Δ_{Fe} isomer has three quite optimal π-stacks similar to the observed *fac*,Λ_{Fe} isomer.‡ However, the three methyl groups point towards each other in the *fac*,Λ_{Fe} isomer causing substantially unfavourable steric interactions. The two *mer* structures are similarly related - the *mer*,Λ_{Fe} contains additional unfavourable steric interactions between two methyl groups pointing towards each other.

The high stability of the *fac*,Δ_{Fe} isomer compared with the other three possible isomers is therefore due to two factors. Firstly, the Δ_{Fe} isomers are favoured due to the lack of unfavourable steric interactions between the methyl groups seen in the Λ_{Fe} structures. Secondly, the three sets of concurrent π-stacks seen exclusively in the *fac* configurations significantly contribute to the stability of the *fac* isomer over the *mer* isomer.

We noted above that during the synthesis of *fac*,Δ_{Fe},*R*$_C$-[Fe$\mathbf{L}^6_3$][ClO$_4$]$_2$ a metastable *mer* isomer was detected. We considered that this kinetic trap may arise as a result of multiple π-stacks involving the benzyl groups, and although a number of such possible structures could be built, these motifs were not conserved in the converged structures.

The synthesis of [Fe$\mathbf{L}^2_3$][ClO$_4$]$_2$ resulted in a thermodynamic product containing a mixture of the (racemic) *fac* and *mer* isomers in a 1 : 2 ratio. The reasons behind the lower selectivity towards the *fac* isomers compared with the chiral ligand complexes, *e.g.* *fac*,Λ_{Fe},*R*$_C$-[Fe$\mathbf{L}^3_3$][ClO$_4$]$_2$, have been investigated as follows.

The substitution of 2-pyridinecarboxaldehyde for 2-acetylpyridine in the standard reaction with benzylamine (**2**) resulted in the formation of the expected *tris* ligand [Fe$\mathbf{L}^{12}_3$][ClO$_4$]$_2$ complex. After 6 h at ambient temperature, the racemic *fac*:*mer* ratio was determined by ^{1}H NMR spectroscopy to be 1 : 6.5. This ratio did not change significantly after 2 d at ambient temperature but on heating the solution to 80 °C for 3 d essentially complete conversion to the *fac* isomers was observed, alongside small amounts of decomposition products.

Fig. 23 depicts our reasoning to account for the unusual substituent steric effects and accompanying π-stacking observed in these compounds. In complexes of $\mathbf{L}^2$, the benzyl group is relatively free to rotate about the N–C bond although, as noted by Busch in related hydrazone complexes, the particular rotamer shown for $\mathbf{L}^2$ in Fig. 23 is untenable.[65] For $\mathbf{L}^3$ the rotamer observed in the molecular structures of the *tris*-complexes is as shown in Fig. 23, with the H atom pointing towards the sterically encumbered region about the Fe atom, and the Ph and Me substituent bonds bifurcated by the imine C–H. This orients the phenyl group rather ideally for π-stacking (*vide supra*), but - as a result of the presence

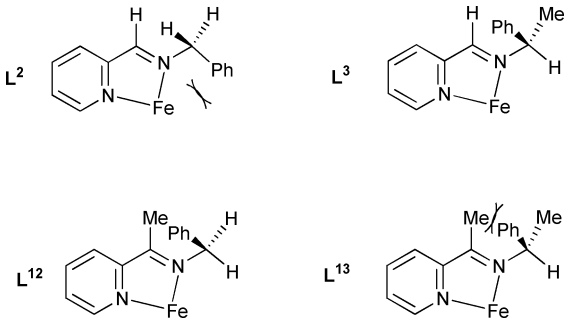

Fig. 23 Steric effects and preferred orientations in complexes of $\mathbf{L}^n$.

of the stereogenic benzylic centre - only towards the reader in Fig. 23 and therefore for the complex only in one helical sense. The ligand $\mathbf{L}^{12}$ is sterically similar to $\mathbf{L}^3$ - both have only one methyl group in the critical region - so the observation of excellent thermodynamic *fac*-selectivity is not unexpected. An explanation for the observation under kinetic control of 1 : 6.5 *fac*:*mer* for the $\mathbf{L}^{12}$ complex is, however, a more complicated issue. The pathway to *mer* isomers is clearly favoured kinetically over *fac*, but the detail of this mechanism of formation is likely to remain unknown. In addition, since the ketimine methyl group in $\mathbf{L}^{12}$ may orient the benzylic phenyl in either direction, this creates the possibility of a number of conformational diastereomers in the *mer* complexes. We do know, however, that while conversion to *fac* is inevitable, the reaction is slow. We thus propose that the preorganising effect that the ketimine methyl group has on the benzyl substituent towards π-stacking is the cause of this kinetic stability and is the reason why the *mer* isomers are observed in the kinetic product. We made a related observation recently in *tris*-ketohydrazone Fe(II) complexes, for which we were able to isolate enantiomerically enriched complexes of achiral ligands with a measured optical $t_{\frac{1}{2}} > 1$ h.[32] Finally, we note that we were unable to detect Fe(II) *tris* complexes of $\mathbf{L}^{13}$, which contains two methyl groups in the imine region.

Conclusions

A range of optically-pure single diastereomer diimine complexes of Fe(II) can be made very readily using 2-pyridinecarboxaldehyde and simple phenylethanamines as the source of chirality. Since these chelate low spin d^6 compounds are relatively inert, stereochemical interconversions are slow - some even on the synthetic timescale - and the diastereomeric ratios can be determined by ^{1}H NMR spectroscopy to be >200 : 1 in all cases.

The origins of this stereoselectivity were investigated *via* NMR spectroscopy, single-crystal X-ray crystallography and DFT calculations. For a given absolute configuration of the phenethanamine unit, one *fac* structure is stabilised by three sets of inter-ligand parallel-offset π-stacking interactions while at the same time avoiding unfavourable steric interactions. The stability of the single *fac* diastereomer is nevertheless finely balanced: similar complexes with other 3*d* metals can be synthesised but do not necessarily show the same degree of diastereoselectivity. While quantification of the stereoselection in the paramagnetic systems is not feasible, the molecular structures of all compounds in the series Mn–Ni, Zn allow a qualitative analysis. The key issue is the M–N bond length, which for Fe(II) places the ligand substituents in essentially

‡ (letters refer to Fig. 19)(a) *fac*,Δ_{Fe},*S*$_C$-[Fe$\mathbf{L}^3_3$]$^{2+}$ *a* = 1.94 Å, *b* = 3.83–3.97 Å, *c* = 3.67–3.84 Å, *d* = 3.48–3.61 Å, *e* = 3.28–3.37 Å, *f* = 3.88–4.10 Å, θ = 15.64–19.71°, φ = 81.81°.(b) *fac*,Λ_{Fe},*S*$_C$-[Fe$\mathbf{L}^3_3$]$^{2+}$ *a* = 1.97 Å, *b* = 3.58–3.69 Å, *c* = 3.44–3.77 Å, *d* = 3.42–3.70 Å, *e* = 3.19–3.40 Å, *f* = 3.68–4.08 Å, θ = 11.84–14.83°, φ = 82.07°.(c) *mer*,Δ_{Fe},*S*$_C$-[Fe$\mathbf{L}^3_3$]$^{2+}$ *a* = 1.95 Å, *b* = 3.45, 3.56 Å, θ = 5.70, 9.46°, φ = 81.84°.(d) *mer*,ΛFe,SC-[Fe$\mathbf{L}^3_3$]$^{2+}$ *a* = 1.96 Å, *b* = 3.38, 3.57 Å, θ = 6.68, 7.24°, φ = 82.56°.

ideal positions for the π-stacking. For diamagnetic Zn(II) the larger radius leads to very weak π-stacking and poorer measured stereoselectivity, although it is proposed that the improvement in diastereoselection with increased solvent polarity may be due to the promotion of this hydrophobic interaction.

In the Fe(II) system, the complex formed with **L**[7] demonstrates that steric effects play an important role alongside the π-stacking, and the *bis*(tridentate) structure formed with **L**[8] reminds us that on the basis of the chelate effect the observation of only the *tris*(bidentate) structure for the Fe(II) complex of **L**[4] is unexpected. Evidently the energetic benefit of the three π-stacks (*ca* 10 kcal mol^{-1}) goes at least some way to offsetting the entropic penalty of retaining the third ligand.

Imidazole-based compounds give similar structures to the pyridines in the solid state and indeed substantial diastereomeric excess in solution, but the complexes are paramagnetic and the actual stereoselectivity is unknown.

The traditional approaches to the isomer problem of tris(bidentate) octahedral structures more commonly use inert metals such as Ru(II) so that racemisation or epimerization rates are negligible. In the current appproach we rely on the accessibility of stereochemical interconversions so that the system is not trapped in some kinetic product mixture (*e.g.* the **L**[6] system) while at the same time ensuring that one isomer is far more thermodynamically stable than the others. As a result only one isomer is present in measurable quantities.

The simplicity and ready accessibility of the stereochemically pure system described here is allowing us to synthesise further derivatives and introduce functionality, which we will report in due course.

Experimental

General considerations

All solvents and chemicals purchased from commercial sources (Sigma-Aldrich, Acros, Fisher Scientific or Alfa Aesar) were used without further purification. Deuterated solvents were purchased from Sigma-Aldrich and Cambridge Isotope Laboratories. Sodium hydride dispersion in mineral oil was placed in a Schlenk vessel under an inert atmosphere and washed three times with diethyl ether to remove the oil. The sodium hydride powder was then dried and stored in the dry box.

Where appropriate, reactions were carried out under argon using a dual manifold argon/vacuum line and standard Schlenk techniques or MBraun dry box. THF was pre-dried over sodium wire and then heated to reflux for 3 d under dinitrogen over potassium and degassed before use. Dried THF was stored in a glass ampoule under argon. All glassware and cannulae were stored in an oven at > 375 K.

NMR spectra were recorded on Bruker Spectrospin 300/400/500 MHz spectrometers. Routine NMR assignments were confirmed by ^{1}H–^{1}H (COSY) and ^{13}C–^{1}H (HMQC) correlation experiments where necessary. The spectra were internally referenced using the residual protio solvent ($CDCl_3$, CD_3CN *etc.*) resonance relative to tetramethylsilane (δ = 0 ppm). ESI mass spectra were recorded on Bruker Esquire 2000 and Bruker MicroTOF spectrometers. Infra-Red spectra were measured using a Perkin-Elmer FTIR spectrometer. Elemental analyses were performed by Warwick Analytical Services, Coventry, UK and MEDAC Ltd, Surrey, UK.

UV-vis absorbance spectra were recorded using a Jasco V-660 spectrometer. Measurements were collected in a 1 cm path-length quartz cuvette and the standard parameters used were: bandwidth 1 nm, response time 1 s, wavelength scan range 200–800 nm, data pitch 0.2 nm, scanning speed 100 nm min^{-1} and accumulation 2. CD spectra were measured on a Jasco J-815 spectrometer, which was calibrated conventionally using 0.060% ACS for intensity and a holmium filter for wavelength, and also against our recently introduced Na[Co(EDDS)] system.[66] Measurements were collected using a 1 cm path-length quartz cuvette and the standard parameters used were: bandwidth 1 nm, response time 1 s, wavelength scan range 200–800 nm, data pitch 0.2 nm, scanning speed 100 nm min^{-1} and accumulation 4.

The crystal data were collected using a Siemens SMART CCD single crystal diffractometer using a Mo-Kα (λ = 0.71073 Å) or Cu-Kα (λ = 1.54184 Å) radiation source. Structures were solved by direct methods using SHELX (TREF)[67,68] with additional light atoms found by Fourier methods. Crystal refinement was performed using SHELX97.[68]

Optical rotation measurements were performed on a Perkin Elmer Polarimeter 341 by Warwick Analytical Services, Coventry, UK. In all cases the following parameters were used: solvent methanol, temperature 20 °C, pathlength 100 mm, wavelength 589 nm.

Magnetic measurements were performed on a Quantum Design MPMS 5S SQuID magnetometer, using an external field of 1000 G in the temperature range 2–400 K. Samples were placed in gelatine capsules. Diamagnetic corrections were calculated using Pascal's constants.[69]

Density functional optimisations were carried out using the Amsterdam Density Functional program (version 2008.01).[64] Starting points for geometry optimisations were taken from crystallographic data where available, and where unavailable, starting structures were created from existing crystallographic fragments. Solution structures were optimised relative to acetonitrile (*vide infra*) using a triple-ζ plus polarisation basis set (TZP) on all atoms with the OPBE functional and Grimme's empirical correction for dispersion.[70] Small frozen cores[71] were used throughout. Calculations used integration level 5 (as defined by ADF) with convergence criteria of e = 0.0001 a.u., rad = 0.005 Å and grad = 0.001 a.u. $Å^{-1}$ for the total binding energy, Cartesian displacement and energy gradient respectively. Acetonitrile solvent effects were included based on the conductor-like screening model (COSMO) implemented in ADF.[72] Non-bonded radii used were H = 1.350 Å, C = 1.700 Å, N = 1.608 Å, Fe = 1.858 Å. A dielectric constant of 37.5 (acetonitrile) and an outer cavity radius of 2.76 Å were further used to parameterise the COSMO solvation cavity.

Synthesis

(*R*)-2-Phenylglycinol (4).

Method 1. (Adapted from prep for (S)-*tert*-Leucinol)[35]

A dry round-bottom Schlenk charged with sodium borohydride (31.21 g, 0.83 mol) and (*R*)-2-phenylglycine (50.00 g, 0.33 mol) was flushed with argon and dry THF (400 mL) was added. The flask was cooled to 0 °C using an ice-water bath before iodine (83.75 g, 0.33 mol) in dry THF (150 mL) was added dropwise

to the solution. A reflux condenser and nitrogen bubbler were fitted and the reaction was stirred at ambient temperature for 2 h, before heating to reflux (80 °C) overnight. Methanol (400 mL) was added slowly until the solution became clear. All solvents were then removed under reduced pressure to leave a white paste, which was dissolved in aqueous 20% potassium hydroxide solution (600 mL) and stirred at ambient temperature overnight. The product was extracted into dichloromethane (5 × 250 mL), dried over sodium sulfate and the solvent removed under reduced pressure to leave the crude product. The product was recrystallised from hot toluene to yield a white crystalline solid. Yield = 23.33 g, 0.17 mol, 52%.

Method 2[34]. Lithium aluminium hydride (4.90 g, 129 mmol, 1.95 eq.) was suspended in dry THF (200 mL) under argon at 0 °C. Solid (*R*)-2-phenylglycine (10.00 g, 66.15 mmol, 1.00 eq.) was added in small portions. The mixture was stirred at 0 °C for 1 h, then slowly heated to reflux (80 °C) overnight. A saturated potassium carbonate solution (75 mL) was added very slowly to the mixture, which was cooled in an ice/water bath. The mixture was filtered and the solvents were removed from the filtrate under reduced pressure. The crude yellow solid was recrystallised from hot toluene to yield a white crystalline solid. Yield 5.74 g, 42 mmol, 63%.

^{1}H NMR (400 MHz, 298 K, $CDCl_3$) δ_H 7.30–7.18 (5H, m, Ph), 3.97 (1H, dd, $^{3}J_{HH}$ = 4.0 Hz, 8.5 Hz, CH), 3.66 (^{1}H, dd, $^{2}J_{HH}$ = 11.0 Hz, $^{3}J_{HH}$ = 4.0 Hz, CH_2), 3.48 (1H, dd, $^{2}J_{HH}$ = 11.0 Hz, $^{3}J_{HH}$ = 8.5 Hz, CH_2), 2.05 (2H, s, NH_2).

^{13}C{^{1}H} NMR (100 MHz, 298 K, $CDCl_3$) δ_C 142.7 (Ph), 128.7 (Ph), 127.5 (Ph), 126.5 (Ph), 68.0 (CH_2), 57.4 (CH).

MS (ESI) *m*/*z* 138.0 $[M+H]^+$, 121.0 $[M–NH_2]^+$.

IR *ν* cm^{-1} 2835 m, 1604 m, 1497 m, 1453 m, 1361 w, 1197 w, 1077 m, 1047 m, 978 m, 882 m, 755 s, 700 s.

Elemental analysis found (calculated for $C_8H_{11}NO$)% C 69.79 (70.04), H 8.08 (8.08), N 10.18 (10.21).

Melting point 76–78 °C (Lit. mp 76–79 °C).[73]

Optical rotation –25.99° (6.619 g/100 mL) [Lit. = –25.8° (6.6 g/100 mL)].[36]

2-Methoxy-1-phenylethanamine (5)[37]**.** (*R*)-2-Phenylglycinol (**4**) (2.00 g, 14.6 mmol, 1.00 eq.) was dissolved in dry THF (20 mL) and was added dropwise to a stirred suspension of sodium hydride (0.72 g, 30.0 mmol, 2.05 eq.) in dry THF (10 mL). The solution was stirred for 1 h at ambient temperature under partial vacuum. Iodomethane (0.96 mL, 15.4 mmol, 1.05 eq.) was added dropwise and the solution was stirred for 1 h at ambient temperature under argon. At this point, the solution was heated to reflux (65 °C) under partial vacuum for a further 2 h before cooling to ambient temperature, followed by the addition of brine (40 mL). The product was extracted into diethyl ether (4 × 60 mL), dried over sodium sulfate and the solvent was removed under reduced pressure to leave a yellow oil (crude yield = 1.80 g). This crude product was purified by Kügelrohr distillation to give a clear oil (bp 70 °C under high vacuum). Purified yield = 1.38 g, 9.1 mmol, 63%.

^{1}H NMR (300 MHz, 298 K, $CDCl_3$) δ_H 7.33–7.16 (5H, m, Ph), 4.12 (1H, dd, $^{3}J_{HH}$ = 4.0 Hz, 9.0 Hz, CH), 3.43 (1H, dd, $^{2}J_{HH}$ = 8.5 Hz, $^{3}J_{HH}$ = 4.0 Hz, CH_2), 3.32–3.26 (4H, m, CH_2, CH_3), 1.67 (2H, s, NH_2).

^{13}C{^{1}H} NMR (75 MHz, 298 K, $CDCl_3$) δ_C 142.6 (Ph), 128.4 (Ph), 127.4 (Ph), 126.8 (Ph), 79.0 (CH_2), 58.9 (CH_3), 55.4 (CH).

MS (ESI) *m*/*z* 135.0 $[M–NH_2]^+$.

IR *ν* cm^{-1} 3028 w, 2888 m, 1603 w, 1493 m, 1453 m, 1355 w, 1194 m, 1111 s, 968 m, 844 m, 758/700 s.

Elemental analysis found (calculated for $C_9H_{13}NO$)% C 71.01 (71.49), H 8.65 (8.67), N 8.92 (9.26).

Optical rotation –34.04° (5.963 g/100 mL).

2-(Benzyloxy)-1-phenylethanamine (6)[38]**.** (*R*)-2-Phenylglycinol (**4**) (1.00 g, 7.3 mmol, 1.00 eq.) was dissolved in dry THF (15 mL) and was added dropwise to a stirred suspension of sodium hydride (0.36 g, 14.9 mmol, 2.05 eq.) in dry THF (10 mL). The solution was stirred for 1 h at ambient temperature under partial vacuum. Benzyl bromide (0.91 mL, 7.7 mmol, 1.05 eq.) was added dropwise over 10 min and the solution was stirred for 1 h at ambient temperature under argon. At this point, the solution was heated to reflux (65 °C) under partial vacuum for a further 3 h before cooling to ambient temperature, followed by the addition of brine (40 mL). The product was extracted into diethyl ether (4 × 60 mL), dried over sodium sulfate and the solvent was removed under reduced pressure to leave a yellow oil (crude yield = 1.42 g). This crude product was purified by two Kügelrohr distillations, the first at 125 °C (under high vacuum) to remove unreacted benzyl bromide and (*R*)-2-phenylglycinol, and the second to give the product, a slightly yellow liquid (bp 165 °C under high vacuum). Purified yield = 0.93 g, 4.1 mmol, 56%.

^{1}H NMR (300 MHz, 298 K, $CDCl_3$) δ_H 7.33–7.16 (10H, m, Ph), 4.49 (2H, s, CH_2Ph), 4.18 (1H, dd, $^{3}J_{HH}$ = 4.0 Hz, 9.0 Hz, CH), 3.54 (1H, dd, $^{2}J_{HH}$ = 9.0 Hz, $^{3}J_{HH}$ = 4.0 Hz, CH_2), 3.38 (1H, t, $^{2}J_{HH}/^{3}J_{HH}$ = 9.0 Hz, CH_2), 1.69 (2H, s, NH_2).

^{13}C{^{1}H} NMR (75 MHz, 298 K, $CDCl_3$) δ_C 142.5 (Ph), 138.2 (Ph), 128.5 (Ph), 127.8 (Ph), 127.7 (Ph), 127.6 (Ph), 127.4 (Ph), 126.9 (Ph), 76.7 (CH_2), 73.3 (CH_2Ph), 55.6 (CH).

MS (ESI) *m*/*z* 228.0 $[M+H]^+$, 250.0 $[M+Na]^+$.

IR *ν* cm^{-1} 3029 w, 2857 w, 1603 w, 1494 m, 1453 m, 1355 w, 1206 w, 1090 s, 1027 m, 843 m, 735 s, 697 s.

Elemental analysis found (calculated for $C_{15}H_{17}NO$)% C 78.88 (79.26), H 7.58 (7.54), N 6.09 (6.16).

Optical rotation –18.87° (3.015 g/100 mL).

***N*-Methyl-1*H*-imidazole-2-carbaldehyde (9)**[39]**.** Methylimidazole (1.0 g, 12.2 mmol) was dissolved in dry THF (20 mL). *n*-Butyllithium (4.5 mL, 2.5 M in hexanes) was added dropwise at –78 °C. The resulting solution was stirred for 1 h, after which dry DMF (2.8 mL, 36.6 mmol) was added and the solution was stirred for a further 3 h. The solution was then warmed to ambient temperature and stirred overnight. The reaction was quenched by the addition of distilled water (20 mL) and extracted into chloroform (3 × 100 mL). The organic layers were combined, dried over sodium sulfate, filtered and the solvent was removed under reduced pressure to give a yellow oil. On cooling to –30 °C a white solid formed and was isolated by filtration and washed with diethyl ether (30 mL) followed by pentane (30 mL) to give the product as a waxy white solid. Yield 1.12 g, 10.17 mmol, 83%.

^{1}H NMR (400 MHz, 298 K, $CDCl_3$) δ_H 9.79 (1H, s, HC═O), 7.24 (1H, s, Imz), 7.08 (1H, s, Imz), 3.99 (3H, s, Me).

^{13}C{^{1}H} NMR (75 MHz, 298 K, $CDCl_3$) δ_C 182.01 (C═O), 143.62 (Imz), 131.36 (Imz), 127.33 (Imz), 34.86 (Me).

MS (ESI) *m*/*z* 111.3 $[M+H]^+$, 133.2 $[M+Na]^+$.

***N-tert*-Butylimidazole[74].** Glyoxal (9.6 g of glyoxal dimer dehydrate, 0.14 mol), *tert*-butylamine (10.0 g, 0.14 mol), methanol (150 mL) and distilled water (25 mL) were heated to 70 °C, at which point formaldehyde (12 mL, 37% aqueous solution, 0.14 mol) was added followed by the dropwise addition of ammonia (10 mL, 28 wt%, 0.14 mol). The resulting solution was stirred for a further 6 h at 70 °C. The solution was cooled to ambient temperature and the solvents were removed under reduced pressure to give a dark yellow oil, which was extracted into dichloromethane (150 mL) and was washed with distilled water (3 × 150 mL). The organic layer was dried over sodium sulfate and the solvent was removed under reduced pressure to give a yellow oil. The product was purified by Kügelrohr distillation to give a colourless oil (bp 70 °C under high vacuum). Yield 8.2 g, 66.0 mmol, 47%.

^{1}H NMR (400 MHz, 298 K, $CDCl_3$) δ_H 7.42 (1H, s, Imz), 6.90 (2H, m, Imz), 1.42 (9H, s, ^{t}Bu).

^{13}C{^{1}H} NMR (75 MHz, 298 K, $CDCl_3$) δ_C 134.0 (Imz), 128.7 (Imz), 116.1 (Imz), 54.4 (^{t}Bu), 30.3 (^{t}Bu).

MS (ESI) *m*/*z* 125.2 $[M+H]^+$, 147.3 $[M+Na]^+$.

***N-tert*-Butyl-1*H*-imidazole-2-carbaldehyde (11).** This compound has previously been synthesised by an alternative method.[75] To a stirred solution of 1-*tert*-butylimidazole (4.0 g, 32.0 mmol) in THF (20 mL) n-butyllithium (20 mL, 2.5 M in hexanes) was added dropwise at −78 °C. The resulting solution was allowed to warm to ambient temperature and stirred for 3 h. Dry DMF (3.0 mL, 38.7 mmol) was added and the resulting yellow solution was stirred overnight. The reaction was quenched by the addition of water (20 mL) and extracted into chloroform (3 × 100 mL). The organic layers were collected and dried over sodium sulfate, filtered and the solvents removed under reduced pressure to give a yellow oil. The product was purified by Kügelrohr distillation to give a colourless oil (70 °C under high vacuum). Yield 3.2 g, 20.0 mmol, 63%.

^{1}H NMR (300 MHz, 298 K, $CDCl_3$) δ_H 9.77 (1H, s, HC═O), 7.34 (1H, d, $^3J_{HH}$ = 1.0 Hz, Imz), 7.23 (1H, d, $^3J_{HH}$ = 1.0 Hz, Imz), 1.65 (9H, s, ^{t}Bu).

^{13}C{^{1}H} NMR (75 MHz, 298 K, $CDCl_3$) δ_C 181.2 (C═O), 144.7 (Imz), 130.5 (Imz), 124.2 (Imz), 58.7 (^{t}Bu), 29.6 (^{t}Bu).

MS (ESI) *m*/*z* 153.2 $[M+H]^+$, 175.2 $[M+Na]^+$.

General procedure for $[FeL^n_3][ClO_4]_2$ complexes (*n* = 1–9,11). 2-Pyridinecarboxaldehyde (3.0 eq.) and iron(II) perchlorate hexahydrate (1.0 eq.) were dissolved in acetonitrile to form a red solution containing the iron(II) *tris*(2-pyridinecarboxaldehyde) complex. The appropriate amine (**1–7**) (3.0 eq.) was added and immediately the solution turned purple. This was stirred overnight before ethyl acetate/diethyl ether was added dropwise until signs of crystallisation. The purple crystals were filtered and dried *in vacuo*. If necessary, the product $[FeL^n_3][ClO_4]_2$, was recrystallised from acetonitrile and ethyl acetate. Yields are unoptimised -analysis of the crude reaction mixtures indicated that reactions were essentially complete. Procedures involving imidazole-2-carbaldehydes were conducted similarly.

$[FeL^1_3][ClO_4]_2$. Yield = 0.67 g, 79%. Ratio is 1 : 15 *fac*:*mer*.

^{1}H NMR (400 MHz, 298 K, CD_3CN) δ_H 9.30 (1H, s, HC═N *mer* isomer), 9.02 (1H, s, CH═N *mer* isomer), 8.88 (0.2H, s, HC═N *fac* isomer), 8.80 (1H, s, HC═N *mer* isomer), 8.54 (1H, d, $^3J_{HH}$ = 9 Hz, Py *mer* isomer), 8.48 (1H, d, $^3J_{HH}$ = 7.5 Hz, Py *mer* isomer), 8.43 (0.2H, d, $^3J_{HH}$ = 9 Hz, Py *fac* isomer), 8.38 (1H, d, $^3J_{HH}$ = 7.5 Hz, Py *mer* isomer), 8.33 (0.2H, t, $^3J_{HH}$ = 9 Hz, Py *fac* isomer), 8.25 (1H, t, $^3J_{HH}$ = 9 Hz, Py *mer* isomer), 8.06 (1H, t, $^3J_{HH}$ = 9 Hz, Py *mer* isomer), 7.94 (3H, m, Py *mer* isomer, 2 × OH *mer* isomer), 7.73 (0.2H, t, $^3J_{HH}$ = 8.5 Hz, Py *fac* isomer), 7.65 (2H, m, 2 × Py *mer* isomer), 7.56 (2H, m, 2 × Py *mer* isomer), 7.48 (2H, m, 2 × Py *mer* isomer), 7.45 (0.2H, s, OH *fac* isomer), 7.43 (0.2H, d, $^3J_{HH}$ = 7.5 Hz, Py *fac* isomer), 7.35 (1H, s, OH *mer* isomer), 6.77 (2H, d, $^3J_{HH}$ = 9.5 Hz, Ph *mer* isomer), 6.68 (0.4H, d, $^3J_{HH}$ = 9.5 Hz, Ph *fac* isomer), 6.58 (6H, m, Ph *mer* isomer), 6.42 (2H, d, $^3J_{HH}$ = 9.5 Hz, Ph *mer* isomer), 6.15 (2H, d, $^3J_{HH}$ = 9.5 Hz, Ph *mer* isomer), 5.54 (0.4H, d, $^3J_{HH}$ = 9.5 Hz, Ph *fac* isomer).

^{13}C {^{1}H} NMR (100 MHz, 298 K, CD_3CN) δ_C 170.8 (C═N), 170.7 (C═N), 170.6 (C═N), 158.8 (Py/Ph), 158.3 (Py/Ph), 158.0 (Py/Ph), 157.5 (Py/Ph), 157.5 (Py/Ph), 157.4 (Py/Ph), 156.7 (Py/Ph), 156.6 (Py), 155.9 (Py), 155.9 (Py), 155.4 (Py/Ph), 155.4 (Py/Ph), 138.6 (Py), 138.3 (Py), 138.2 (Py), 131.0 (Py), 129.7 (Py), 129.3 (Py), 128.6 (Py), 128.2 (Py), 128.1 (Py), 123.7 (Ph), 123.2 (Ph), 123.2 (Ph), 116.0 (Ph), 115.6 (Ph), 115.2 (Ph). All labelled peaks are the *mer* isomer. The *fac* isomer is too weak to distinguish.

MS (ESI) *m*/*z* 199.2 $[L+H]^+$.

IR ν cm^{-1}: 3327 w, 1592 m, 1507 m, 1473 m, 1448 m, 1354 w, 1275 m, 1226 m, 1042 s, 834 m, 767 s.

Elemental analysis found (calculated for $C_{36}H_{30}O_{11}Cl_2FeN_6$)% C 50.13 (50.90), H 3.61 (3.56), N 9.51 (9.89).

$[FeL^2_3][ClO_4]_2 \cdot \frac{1}{2}CH_3CN$. Yield = 26%. Ratio is 1 : 2 *fac*:*mer*.

^{1}H NMR (400 MHz, 298 K, CD_3CN) δ_H 9.08 (1H, s, CH═N *mer*), 8.49 (3H, s, CH═N *fac*), 8.38 (1H, s, CH═N *mer*), 8.30 (2H, m, Py *mer*), 8.22 (1H, s, CH═N, *mer*), 8.17 (1H, t, $^3J_{HH}$ = 7.0 Hz, Py *mer*), 8.02 (1H, t, $^3J_{HH}$ = 7.0 Hz, Py *mer*), 7.98-6.80 (50H, m, Py/Ph *mer* and *fac*), 5.48 (3H, d, $^2J_{HH}$ = 12.5 Hz, CH_2 *fac*), 5.38 (1H, d, $^2J_{HH}$ = 12.5 Hz, CH_2 *mer*), 5.06 (3H, d, $^2J_{HH}$ = 12.5 Hz, CH_2 *fac*), 4.94 (1H, d, $^2J_{HH}$ = 12.5 Hz, CH_2 *mer*), 4.81 (1H, d, $^2J_{HH}$ = 12.5 Hz, CH_2 *mer*), 4.49 (1H, d, $^2J_{HH}$ = 12.5 Hz, CH_2 *mer*), 4.38 (1H, d, $^2J_{HH}$ = 12.5 Hz, CH_2 *mer*), 4.07 (1H, d, $^2J_{HH}$ = 12.5 Hz, CH_2 *mer*).

^{13}C{^{1}H} NMR (100 MHz, 298 K, CD_3CN) δ_C 174.0 (C═N), 153.7 (Py/Ph), 138.2 (Py/Ph), 128.9 (Py/Ph), 128.9 (Py/Ph), 128.7 (Py/Ph), 128.6 (Py/Ph), 128.1 (Py/Ph), 127.9 (Py/Ph), 126.9 (Py/Ph), 65.2 (CH_2), 64.4 (CH_2), 63.6 (CH_2), 62.6 (CH_2). Many peaks due to the same carbon in the *fac*/*mer* isomers overlap.

MS (ESI) *m*/*z* 322.1 $[FeL^2_3]^{2+}$.

IR ν cm^{-1} 1614 w, 1590 w, 1556 w, 1496 m, 1471 m, 1444 m, 1297 w, 1239 w, 1072 s, 741 s, 698 s, 622 s.

Elemental analysis found (calculated for $C_{40}H_{37.5}Cl_2FeN_{6.5}O_8$)% C 55.22 (55.60), H 4.39 (4.37), N 10.59 (10.54).

***fac*,Λ_{Fe},*R*$_C$-$[FeL^3_3][ClO_4]_2$.** Yield = 64%.

^{1}H NMR (400 MHz, 298 K, CD_3CN) δ_H 8.75 (3H, s, HC═N), 7.83 (3H, t, $^3J_{HH}$ = 7.0 Hz, Py), 7.47 (3H, d, $^3J_{HH}$ = 7.0 Hz, Py), 7.33 (3H, t, $^3J_{HH}$ = 7.0 Hz, Py), 7.12 (3H, t, $^3J_{HH}$ = 8.5 Hz, Ph), 6.99 (6H, t, $^3J_{HH}$ = 8.5 Hz, Ph), 6.74 (3H, d, $^3J_{HH}$ = 7.0 Hz, Py), 6.59 (6H, d, $^3J_{HH}$ = 8.5 Hz, Ph), 5.36 (3H, quartet, $^3J_{HH}$ = 4.0 Hz, CH), 1.98 (9H, d, $^3J_{HH}$ = 4.0 Hz, CH_3).

^{13}C{^{1}H} NMR (100 MHz, 298 K, CD_3CN) δ_C 170.8 (C═N), 158.2 (Py), 153.6 (Py), 139.5 (Ph), 138.3 (Py), 129.1 (Py), 129.0 (Ph), 127.8 (Py), 127.3 (Ph), 124.4 (Ph), 69.1 (CH), 25.4 (CH_3).

MS (ESI) *m*/*z* 343.14 $[FeL^3_3]^{2+}$.

IR ν cm^{-1} 1706 m, 1614 w, 1444 m, 1386 w, 1070 s, 757 s, 701 s.

Elemental analysis found (calculated for $C_{42}H_{42}Cl_2FeN_6O_8$)% C 56.81 (56.96), H 5.02 (4.78), N 9.08 (9.49).

The *fac*,Δ_{Fe},S_C isomer was prepared similarly.

***fac*,Δ_{Fe},R_C-[FeL$^4_3$][ClO$_4$]$_2$·$\frac{1}{2}$CH$_3$CN·$\frac{1}{4}$H$_2$O.** Yield = 47%.

^{1}H NMR (400 MHz, 298 K, CD_3CN) δ_H 8.97 (3H, s, HC═N), 7.73 (3H, t, $^3J_{HH}$ = 7.0 Hz, Py), 7.42 (3H, d, $^3J_{HH}$ = 7.0 Hz, Py), 7.21 (3H, t, $^3J_{HH}$ = 7.0 Hz, Py), 7.11 (3H, t, $^3J_{HH}$ = 8.5 Hz, Ph), 7.00 (6H, t, $^3J_{HH}$ = 8.5 Hz, Ph), 6.82 (9H, m, Py/Ph), 5.77 (3H, dd, $^3J_{HH}$ = 11.0 Hz, $^3J_{HH}$ = 1.5 Hz, CH), 4.26 (3H, m, CH_2), 4.10 (3H, m, OH), 3.92 (3H, m, CH_2).

^{13}C{^{1}H} NMR (100 MHz, 298 K, CD_3CN) δ_C 171.4 (C═N), 158.6 (Py), 153.4 (Py), 138.2 (Py), 135.1 (Ph), 128.7 (Py), 128.5 (Ph), 127.6 (Ph), 127.4 (Py), 125.7 (Ph), 73.3 (CH), 64.6 (CH_2).

MS (ESI) *m*/*z* 607.10 [(FeL$^4_2$)(ClO$_4$)]$^+$.

IR *ν* cm^{-1} 3463 w, 1614 w, 1473 m, 1452 m, 1241 w, 1080 s, 757 s, 701 s.

Elemental analysis found (calculated for $C_{43}H_{44}Cl_2FeN_{6.5}O_{11.25}$)% C 53.30 (53.88), H 4.57 (4.63), N 9.34 (9.50).

Crystallography (CCDC refcode COWFAW[31]):

fac,Δ_{Fe},R_C-[FeL$^4_3$][ClO$_4$]$_2$·$\frac{1}{2}$CH$_3$CN·$\frac{1}{4}$H$_2$O $C_{43}H_{44}Cl_2FeN_{6.5}O_{11.25}$, M_r = 958.60, monoclinic, $P2_1$, pink plate 0.30 × 0.20 × 0.02 mm, a = 18.5532(6), b = 12.1579(2), c = 19.1141(6) Å, α = 90°, β = 90.7860(10)°, γ = 90°, U = 4311.1(2) Å^3, Z = 4, T = 120(2) K, radiation Mo-Kα (λ = 0.71073 Å), 44 867 total reflections, 15 037 unique (R_{int} = 0.1029), R_1 = 0.0557 (obs. data), wR_2 = 0.1209 (all data), GooF 1.012, Flack 0.004(16).

***fac*,Δ_{Fe},R_C-[FeL$^5_3$][ClO$_4$]$_2$·2CH$_3$CN.** Yield = 75%.

^{1}H NMR (400 MHz, 298 K, CD_3CN) δ_H 8.89 (3H, s, HC═N), 7.69 (3H, td, $^3J_{HH}$ = 7.5 Hz, $^4J_{HH}$ = 1.5 Hz, Py), 7.38 (3H, d, $^3J_{HH}$ = 7.5 Hz, Py), 7.17 (3H, m, Py), 7.09 (3H, t, $^3J_{HH}$ = 7.5 Hz, Ph), 6.98 (6H, t, $^3J_{HH}$ = 7.5 Hz, Ph), 6.77 (3H, d, $^3J_{HH}$ = 5.5 Hz, Py), 6.71 (6H, d, $^3J_{HH}$ = 7.5 Hz, Ph), 5.81 (3H, dd, $^3J_{HH}$ = 3.5 Hz, 10.5 Hz, CH), 4.23 (3H, t, $^2J_{HH}$/$^3J_{HH}$ = 10.5 Hz, CH_2), 3.67 (9H, s, CH_3), 3.55 (3H, dd,$^2J_{HH}$ = 10.5 Hz, $^3J_{HH}$ = 3.5 Hz, CH_2).

^{13}C{^{1}H} NMR (100 MHz, 298 K, CD_3CN) δ_C 171.1 (C═N), 158.5 (Py), 153.5 (Py), 138.3 (Py), 134.7 (Ph), 129.0 (Py), 128.9 (Ph), 127.8 (Ph), 127.5 (Py), 125.6 (Ph), 74.0 (CH_2), 70.9 (CH), 58.2 (CH_3).

MS (ESI) *m*/*z* 388.16 [FeL$^5_3$]$^{2+}$, 635.14 [(FeL$^5_2$)(ClO$_4$)]$^+$.

IR *ν* cm^{-1} 1613 w, 1473 m, 1451 m, 1236 w, 1078 s, 758 s, 699 s.

Elemental analysis found (calculated for $C_{49}H_{54}Cl_2FeN_8O_{11}$)% C 55.29 (55.64), H 4.89 (5.15), N 10.12 (10.59).

Crystallography:

fac,Δ_{Fe},R_C-[FeL$^5_3$][ClO$_4$]$_2$·2CH$_3$CN $C_{49}H_{54}Cl_2FeN_8O_{11}$, M_r = 1057.75, orthorhombic, $P2_12_12_1$, purple block 0.14 × 0.06 × 0.05 mm, a = 13.2870(4), b = 18.8293(7), c = 20.0225(8) Å, α = 90°, β = 90°, γ = 90°, U = 5009.3(3) Å^3, Z = 4, T = 120(2) K, radiation Mo-Kα (λ = 0.71073 Å), 25 270 total reflections, 8665 unique (R_{int} = 0.1236), R_1 = 0.0869 (obs. data), wR_2 = 0.2018 (all data), GooF 1.118, Flack 0.09(4).

***fac*,Δ_{Fe},R_C-[FeL$^6_3$][ClO$_4$]$_2$·CH$_3$CN.** Yield = 36%

^{1}H NMR (400 MHz, 298 K, CD_3CN) δ_H 8.88 (3H, s, HC═N), 7.68–7.61 (9H, m, Py/Ph), 7.42–7.31 (12H, m, Py/Ph), 7.12 (3H, t, $^3J_{HH}$ = 6.5 Hz, Py), 7.02 (3H, t, $^3J_{HH}$ = 7.0 Hz, Ph), 6.86 (6H, t, $^3J_{HH}$ = 7.0 Hz, Ph), 6.68 (3H, d, $^3J_{HH}$ = 6.5 Hz, Py), 6.53 (6H, d, $^3J_{HH}$ = 7.0 Hz, Ph), 5.74 (6H, dd, $^3J_{HH}$ = 10.0 Hz, $^3J_{HH}$ = 3.0 Hz, CH), 4.79 (3H, d, $^2J_{HH}$ = 11.0 Hz, CH_2Ph), 4.76 (3H, d, $^2J_{HH}$ = 11.0 Hz, CH_2Ph), 4.14 (3H, t, $^2J_{HH}$/$^3J_{HH}$ = 10.0 Hz, CH_2), 3.28 (3H, dd, $^3J_{HH}$ = 9.5 Hz, $^3J_{HH}$ = 3.0 Hz, CH_2).

^{13}C{^{1}H} NMR (100 MHz, 298 K, CD_3CN) δ_C 171.0 (C═N), 158.5 (Ph/Py), 153.4 (Py), 138.3 (Ph/Py), 137.5 (Ph/Py), 134.6 (Ph/Py), 128.9 (Ph/Py), 128.8 (Ph/Py), 128.6 (Ph/Py), 128.4 (Ph/Py), 128.2 (Ph/Py), 127.8 (Ph/Py), 127.4 (Ph/Py), 125.8 (Ph), 73.5 (CH_2Ph), 72.1 (CH*C*H$_2$), 71.1 (CH).

MS (ESI) *m*/*z* 502.20 [FeL$^6_3$]$^{2+}$.

IR *ν* cm^{-1} 1613 w, 1454 m, 1362 w, 1241 w, 1084 s, 758 s, 701 s.

Elemental analysis found (calculated for $C_{65}H_{63}Cl_2FeN_7O_{11}$)% C 62.85 (62.71), H 4.99 (5.10), N 7.67 (7.88).

Λ_{Fe},R_C-[FeL$^7_3$][ClO$_4$]$_2$·H$_2$O. Yield = 24%. Ratio is 2.6 : 1 *fac*:*mer*.

^{1}H NMR (400 MHz, 298 K, CD_3CN) δ_H 9.32 (1H, s, HC═N, *mer*), 9.25 (1H, s, HC═N, *mer*), 9.00 (1H, s, HC═N, *mer*), 8.91 (3H, s, HC═N, *fac*), 8.43–7.45 (21H, m, Py *mer*/*fac*), 6.85 (3H, d, $^3J_{HH}$ = 6.0 Hz, Py, *fac*), 3.89 (3H, m, CH, *fac*), 3.59 (1H, m, CH *mer*), 3.45 (1H, m, CH *mer*), 3.27 (1H, m, CH *mer*), 1.66–0.54 (84H, m, CH_3/Cy, *mer*/*fac*).

^{13}C{^{1}H} NMR (100 MHz, 298 K, CD_3CN) δ_C 170.3 (C═N), 159.3 (Py), 154.6 (Py), 138.9 (Py), 129.8 (Py), 128.3 (Py), 69.2 (CH), 40.5 (CH_3), 30.8 (Cy), 26.3 (Cy), 25.6 (Cy), 23.4 (Cy).

All peaks on ^{13}C {^{1}H} NMR are due to the major isomer (*fac*,Λ). The peaks for the *mer*,Λ isomer are too small to be observed.

MS (ESI) *m*/*z* 352.21 [FeL$^7_3$]$^{2+}$.

IR *ν* cm^{-1} 1731 w, 1612 w, 1445 m, 1395 w, 1241 m, 1077 s, 766 m.

Elemental analysis found (calculated for $C_{42}H_{62}Cl_2FeN_6O_9$)% C 55.03 (54.73), H 6.67 (6.78), N 8.89 (9.12).

***mer*,S_C-[FeL$^8_2$][ClO$_4$]$_2$.** Despite the stoichiometry used, analysis indicated that only two ligands were coordinated to each iron(II) centre. Yield = 0.28 g, 0.42 mmol, 63%.

MS (ESI) *m*/*z* 207.15 [L^8+H]$^+$.

IR *ν* cm^{-1} 3225 w, 1600 m, 1481 m, 1370 m, 1225 m, 1046 s, 786 s.

Elemental analysis found (calculated for $C_{24}H_{36}Cl_2FeN_4O_{10}$)% C 43.48 (43.20), H 5.46 (5.44), N 8.59 (8.40).

Crystallography (CCDC refcode COWFEA[31]):

mer,S_C-[FeL$^8_2$][ClO$_4$]$_2$ $C_{24}H_{36}Cl_2FeN_4O_{10}$, M_r = 667.32, monoclinic, $P2_1$, red block 0.16 × 0.15 × 0.13 mm, a = 9.5751(2), b = 15.1762(3), c = 10.7704(2) Å, α = 90°, β = 110.5290(10)°, γ = 90°, U = 1465.69(5) Å^3, Z = 2, T = 120(2) K, radiation Mo-Kα (λ = 0.71073 Å), 16 635 total reflections, 6382 unique (R_{int} = 0.0313), R_1 = 0.0269 (obs. data), wR_2 = 0.0654 (all data), GooF 1.046, Flack 0.006(12).

[FeL$^9_3$][ClO$_4$]$_2$·$\frac{1}{2}$CH$_3$CN. Yield 0.42 g, 0.46 mmol, 51%.

Elemental analysis found (calculated for $C_{40}H_{46.50}Cl_2FeN_{9.50}O_8$)% C 52.38 (52.50), H 5.33 (5.12), N 14.60 (14.54).

IR *ν* cm^{-1} 3152 w, 1577 m, 1454 m, 1425 m, 1290 m, 1181 w, 1025 s.

Crystallography:

fac,Λ_{Fe},R_C-[FeL$^9_3$][ClO$_4$]$_2$·$\frac{1}{2}$CH$_3$CN $C_{40}H_{46.50}Cl_2FeN_{9.50}O_8$, M_r = 915.12, Monoclinic, $P2_1$, purple block 0.20 × 0.15 × 0.15 mm, a = 12.2800(3), b = 17.6405(4), c = 20.8359(5) Å, α = 90°, β = 92.794(2)°, γ = 90°, U = 4508.20(19) Å^3, Z = 4, T = 298(2) K, radiation Cu-Kα (λ = 1.54184 Å), 15 340 total reflections, 10 206

unique (R_{int} = 0.0270), R_1 = 0.0470 (obs. data), wR_2 = 0.1337 (all data), GooF 1.071, Flack 0.005(4).

[FeL$^{11}_3$][ClO$_4$]$_2$1.25(CH$_3$CN). Yield = 0.42 g, 0.39 mmol, 65%. Elemental analysis found (calculated for $C_{50.50}H_{66.75}Cl_2FeN_{10.25}O_8$)% C 56.03 (56.57), H 6.07 (6.28), N 12.01 (13.39).

UV-vis in CH_3CN (λ, nm; ε, M^{-1} cm^{-1}) 274 (30333), 536 (2117).

IR ν cm^{-1} 2984 w, 1731 m, 1558 m, 1441 m, 1373 m, 1264 m, 1234 m, 1159 m, 1078 s, 915 w, 846 w.

Crystallography:

fac,Λ_{Fe},R_C-[FeL$^{11}_3$][ClO$_4$]$_2$·1.25(CH_3CN) $C_{50.50}H_{66.75}Cl_2FeN_{10.25}O_8$, M_r = 1072.14, Orthorhombic, $P2_12_12_1$, purple block 0.40 × 0.20 × 0.15 mm, a = 12.0388(4), b = 17.7032(6), c = 25.8524(6) Å, α = 90°, β = 90°, γ = 90°, U = 5509.8(3) Å^3, Z = 4, T = 100(2) K, radiation Mo-Kα (λ = 0.71073 Å), 33 650 total reflections, 15 181 unique (R_{int} = 0.0563), R_1 = 0.0580 (obs. data), wR_2 = 0.1424 (all data), GooF 0.814, Flack 0.001(17).

***fac*-[FeL$^{12}_3$][ClO$_4$]$_2$.** 2-Acetylpyridine (0.34 mL, 3.0 mmol, 3.0 eq.) and iron(II) perchlorate hexahydrate (0.36 g, 1.0 mmol, 1.0 eq.) were dissolved in acetonitrile to form a red solution containing the iron(II) *tris*(2-acetylpyridine) complex. Benzylamine (**2**) (0.33 mL, 3.0 mmol, 3.0 eq.) was added and immediately the solution turned purple. This was stirred for 6 h at ambient temperature and a ^{1}H NMR spectrum was measured for a sample of the crude reaction mixture (1 : 6.5 *fac*:*mer*). The solution was stirred for a further 2 d at ambient temperature and a ^{1}H NMR spectrum was measured for a second sample of the crude reaction mixture (1 : 6.5 *fac*:*mer*). The solution was then stirred at 80 °C for 3 d. A ^{1}H NMR spectrum measured for a sample of the crude reaction mixture after this time showed the *fac*-isomer exclusively (with a small amount of decomposition).

^{1}H NMR (300 MHz, 298 K, CD_3CN) δ_H 7.88 (3H, td, $^3J_{HH}$ = 7.5 Hz, $^4J_{HH}$ = 1.0 Hz, Py), 7.56 (3H, d, $^3J_{HH}$ = 7.5 Hz, Py), 7.38 (3H, t, $^3J_{HH}$ = 5.5 Hz, Py), 7.10 (3H, t, $^3J_{HH}$ = 7.5 Hz, Ph), 6.95 (6H, t, $^3J_{HH}$ = 7.5 Hz, Ph), 6.76 (3H, d, $^3J_{HH}$ = 5.5 Hz, Py), 6.42 (6H, d, $^3J_{HH}$ = 7.5 Hz, Ph), 5.68 (3H, d, $^2J_{HH}$ = 15.0 Hz, CH_2), 4.88 (3H, d, $^2J_{HH}$ = 15.0 Hz, CH_2), 2.35 (9H, s, CH_3).

^{13}C{^{1}H} NMR (75 MHz, 298 K, CD_3CN) δ_C 154.6 (Py/Ph), 138.9 (Py/Ph), 134.2 (Py/Ph/ketimine), 130.1 (Py/Ph/ketimine), 129.8 (Py/Ph), 129.1 (Py/Ph), 128.6 (Py/Ph), 128.2 (Py/Ph), 127.2 (Py/Ph/ketimine), 126.0 (Py/Ph), 60.6 (CH_2), 18.1 (CH_3).

MS (ESI) m/z 343.1 [FeL$^{12}_3$]$^{2+}$.

IR ν cm^{-1} 1602 w, 1496 w, 1472 w, 1453 w, 1379 w, 1330 w, 1256 w, 1080 s, 929 w, 770 m, 741 m, 701 m.

Elemental analysis found (calculated for $C_{42}H_{42}Cl_2N_6O_8$)% C 56.41 (56.96), H 4.63 (4.78), N 9.26 (9.49).

General procedure for [ZnL$^3_3$][BF$_4$]$_2$ and [ZnL$^4_2$][BF$_4$]$_2$ Complexes. 2-Pyridinecarboxaldehyde (3.0 eq.) and the appropriate amine (**3**,**4**) (3.0 eq.) were dissolved in acetonitrile to form a yellow solution containing the ligand. Zinc(II) tetrafluoroborate hydrate (H_2O = 6–7) (1.0 eq.) was added and no colour change was observed. This solution was stirred overnight at ambient temperature before ethyl acetate/diethyl ether was added dropwise until signs of crystallisation. The white crystals were filtered and dried *in vacuo*. Yields are unoptimised - analysis of the crude reaction mixtures indicates that reactions are essentially complete.

Λ_{Zn},R_C-[ZnL$^3_3$][BF$_4$]$_2$. Yield = 26%. Ratio is 6.5 : 1 *fac*:*mer*.

^{1}H NMR (400 MHz, 298 K, CD_3CN) δ_H 8.21 (3H, s, HC═N), 8.07 (3H, td, $^3J_{HH}$ = 8.0 Hz, $^4J_{HH}$ = 2 Hz, Py), 7.53 (3H, m, Py), 7.45 (3H, d, $^3J_{HH}$ = 8.0 Hz, Py), 7.40 (3H, d, $^3J_{HH}$ = 5.5 Hz, Py), 7.09 (3H, t, $^3J_{HH}$ = 7.0 Hz, Ph), 6.92 (6H, t, $^3J_{HH}$ = 7.0 Hz, Ph), 6.63 (6H, d, $^3J_{HH}$ = 7.0 Hz, Ph), 5.45 (3H, quartet, $^3J_{HH}$ = 7.5 Hz, CH), 1.62 (9H, d, $^3J_{HH}$ = 7.5 Hz, CH_3).

These are the major peaks observed, which correspond to the *fac*,Λ isomer. There are also small broad peaks corresponding to the peaks observed for the *mer*,Λ isomer, which sharpen at lower temperatures.

^{13}C{^{1}H} NMR (100 MHz, 298 K, CD_3CN) δ_C 161.6 (C═N), 147.6 (Py), 146.1 (Ph/Py), 141.4 (Py), 140.4 (Ph/Py), 129.9 (Ph/Py), 129.2 (Ph/Py), 128.7 (Ph/Py), 127.6 (Ph), 125.5 (Ph), 64.1 (CH), 22.6 (CH_3).

All peaks on ^{13}C{^{1}H} NMR spectrum are from the major isomer (*fac*,Λ). The peaks for the *mer*,Λ isomer are too weak to be observed.

MS (ESI) m/z 211.0 [L^3+H]$^+$.

IR ν cm^{-1} 1647 w, 1598 m, 1446 m, 1392 w, 1050 s, 761 s, 702 s.

Elemental analysis found (calculated for $C_{42}H_{42}B_2F_8N_6Zn$)% C 57.51 (57.99), H 4.91 (4.87), N 9.47 (9.66).

Crystallography:

fac,Λ_{Zn},R_C-[ZnL$^3_3$][ClO$_4$]$_2$·CH_3CN·EtOAc $C_{48}H_{53}Cl_2N_7O_{10}Zn$, M_r = 1024.24, monoclinic, $P2_1$, colourless block 0.35 × 0.35 × 0.20 mm, a = 12.12947(12), b = 13.37998(12), c = 15.44345(15) Å, α = 90°, β = 103.3800(10)°, γ = 90°, U = 2438.32(4) Å^3, Z = 2, T = 100(2) K, radiation Cu-Kα (λ = 1.54184 Å), 49 726 total reflections, 9264 unique (R_{int} = 0.0421), R_1 = 0.0487 (obs. data), wR_2 = 0.1323 (all data), GooF 1.045, Flack 0.007(14).

R_C-[ZnL$^4_2$][BF$_4$]$_2$. MS (ESI) m/z 227.1 [L^4+H]$^+$.

IR ν cm^{-1} 1661 m, 1604 m, 1447 w, 1313 m, 1219 w, 1050 s, 773 s, 705 s.

Elemental analysis found (calculated for $C_{28}H_{28}B_2F_8N_4O_2Zn$)% C 48.48 (48.63), H 4.08 (4.08), N 8.05 (8.10).

R_C-[CoL$^3_3$][PF$_6$]$_2$·2MeOH. Ligand L^3 (0.50 g, 2.38 mmol, 3.0 eq.) was dissolved in methanol (25 mL) and stirred at ambient temperature as cobalt(II) chloride (0.10 g, 0.79 mmol, 1.0 eq.) in methanol (5 mL) was added causing an immediate colour change from yellow to orange. The solution was stirred at ambient temperature for 2 h. A solution of $NaPF_6$ in water (2 mL) was added, causing the immediate formation of an orange precipitate. The precipitate was filtered, washed with methanol and dried *in vacuo*. Yield = 0.55 g, 0.53 mmol, 67%.

MS (ESI) m/z 344.64 [CoL$^3_3$]$^{2+}$.

IR ν cm^{-1} 1639 w, 1598 w, 1494 w, 1446 w, 1391 w, 1321 w, 1234 w, 1162 w, 1113 w, 1072 w, 1019 w, 982 w, 925 w, 829 s, 780 m, 760 m, 702 m.

Elemental analysis found (calculated for $C_{44}H_{50}CoF_{12}N_6O_2P_2$)% C 50.04 (50.63), H 4.31 (4.83), N 8.29 (8.05).

Crystallography:

fac,Λ_{Co},R_C-[CoL$^3_3$][PF$_6$]$_2$·2MeOH $C_{44}H_{50}CoF_{12}N_6O_2P_2$, M_r = 1043.77, monoclinic, $P2_1$, yellow block 0.26 × 0.15 × 0.09 mm, a = 11.6650(5), b = 13.5956(5), c = 15.3936(7) Å, α = 90°, β = 95.949(2)°, γ = 90°, U = 2428.16(18) Å^3, Z = 2, T = 120(2) K, radiation Mo-Kα (λ = 0.71073 Å), 33 640 total reflections, 11 096 unique (R_{int} = 0.0782), R_1 = 0.0669 (obs. data), wR_2 = 0.1828 (all data), GooF 0.986, Flack 0.044(18).

***S*$_C$-[CoL$^3_3$][PF$_6$]$_3$·3CH$_3$CN.** The solvents were degassed before use. The ligand and $Na_3[Co(NO_2)_6]$ were dried *in vacuo* for 2 h before use. Ligand **L^3** (0.50 g, 2.38 mmol, 3.0 eq.) was dissolved in a mixture of acetonitrile (40 mL) and water (3 mL). $Na_3[Co(NO_2)_6]$ (0.32 g, 0.79 mmol, 1.0 eq.) was added as a solid and immediately the colour changed to orange. The solution was stirred overnight at ambient temperature and then sodium perchlorate (0.29 g, 2.38 mmol, 3.0 eq.) was added, and the solution was stirred for a further 4 h at ambient temperature. After this time the solvent was removed under reduced pressure and the resulting crude solid was dissolved in DCM (60 mL) and washed with water (15 mL). The DCM layer was concentrated until signs of precipitation were observed (*ca* 10 mL). The resulting precipitate was filtered and dried *in vacuo*. Yield = 0.17 g, 0.14 mmol, 17%.

This complex was found to be unstable and decomposed rapidly thus preventing detailed analysis on a pure sample.

Crystallography:

fac,Δ_{Co},*S*$_C$-[CoL$^3_3$][PF$_6$]$_3$·3CH$_3$CN $C_{48}H_{51}CoF_{18}N_9P_3$, M_r = 1247.82, monoclinic, $P2_1$, pink plate 0.16 × 0.06 × 0.02 mm, a = 11.978, b = 11.769, c = 18.739 Å, α = 90°, β = 92.09°, γ = 90°, U = 2639.9 Å^3, Z = 2, T = 120(2) K, radiation Mo-Kα (λ = 0.71073 Å), 47 585 total reflections, 11 835 unique (R_{int} = 0.0919), R_1 = 0.0669 (obs. data), wR_2 = 0.1382 (all data), GooF 1.170, Flack 0.08(1).

***S*$_C$-[NiL$^3_3$][ClO$_4$]$_2$·CH$_3$CN·EtOAc.** 2-Pyridinecarboxaldehyde (0.88 g, 8.19 mmol, 3 eq.) and (*S*)-α-methylbenzylamine (0.99 g, 8.19 mmol, 3 eq.) were dissolved in acetonitrile (10 mL) and stirred at ambient temperature for 30 min. A solution of $Ni(ClO_4)_2·6H_2O$ (1.00 g, 2.73 mmol, 1 eq.) in acetonitrile (5 mL) was added resulting in a red solution. The reaction was stirred for a further 2 h before ethyl acetate was added dropwise. The product was left to crystallise overnight. The red/brown crystals were collected by vacuum filtration and dried in air. Yield 1.59 g, 1.56 mmol, 57%.

MS (ESI) m/z 344.1 [NiL$^3_3$]$^{2+}$, 239.1 [NiL$^3_2$]$^{2+}$.

IR ν cm^{-1} 1736 w, 1641 w, 1599 m, 1493 w, 1446 w, 1390 w, 1373 w, 1320 w, 1235 w, 1082 s, 1019 w, 982 w, 925 w, 779 w, 760 m, 702 m.

Elemental analysis found (calculated for $C_{48}H_{53}Cl_2N_7NiO_{10}$)% C 56.66 (56.66), H 5.35 (5.25), N 10.34 (9.64).

Crystallography:

fac,Δ_{Ni},*S*$_C$-[NiL$^3_3$][ClO$_4$]$_2$·CH$_3$CN·EtOAc $C_{48}H_{53}Cl_2N_7NiO_{10}$, M_r = 1017.58, monoclinic, $P2_1$, red block 0.25 × 0.25 × 0.20 mm, a = 12.1724(3), b = 13.3579(2), c = 15.4379(3) Å, α = 90°, β = 103.8310(10)°, γ = 90°, U = 2437.38(8) Å^3, Z = 2, T = 120(2) K, radiation Mo-Kα (λ = 0.71073 Å), 28 903 total reflections, 11 043 unique (R_{int} = 0.0445), R_1 = 0.0515 (obs. data), wR_2 = 0.1258 (all data), GooF 1.055, Flack 0.044(11).

***R*$_C$-[MnL$^3_3$][ClO$_4$]$_2$·2CH$_3$CN.** $Mn(ClO_4)_2·6H_2O$ (0.15 g, 0.4 mmol) was add to a stirred solution of 2-pyridinecarboxaldehyde (0.14 g, 1.3 mmol) and (*R*)-α-methylbenzylamine (0.16 mL, 1.3 mmol) in acetonitrile (20 mL) at ambient temperature and stirred for 4 h. The resulting yellow solution yielded the desired product as a yellow crystalline solid on the addition of ethyl acetate. Yield 66%.

Elemental analysis found (calculated for $C_{46}H_{48}Cl_2MnN_8O_8$)% C 57.50 (57.15), H 5.10 (5.00), N 11.20 (11.59).

IR ν cm^{-1} 2993 w, 2287 w, 2249 w, 1981 w, 1641 m, 1597 m, 1494 m, 1483 w, 1443 m, 1392 m, 1324 m, 1272c w, 1232 w, 1072 s, 1101 s, 983 m, 921 m, 782 m,757 s.

Crystallography:

fac,Λ_{Mn},*R*$_C$-[MnL$^3_3$][ClO$_4$]$_2$·2CH$_3$CN $C_{46}H_{48}Cl_2MnN_8O_8$, M_r = 966.76, orthorhombic, $P2_12_12_1$, yellow block 0.30 × 0.20 × 0.20 mm, a = 13.9695(2), b = 17.3214(3), c = 19.2264(3) Å, α = 90°, β = 90°, γ = 90°, U = 4652.23(12) Å^3, Z = 4, T = 100(2) K, radiation Mo-Kα (λ = 0.71073 Å), 54 447 total reflections, 12 920 unique (R_{int} = 0.0522), R_1 = 0.0591 (obs. data), wR_2 = 0.1292 (all data), GooF 1.078, Flack 0.038(16).

Acknowledgements

The Oxford Diffraction Gemini XRD system was obtained through the Science City Advanced Materials project: Creating and Characterising Next Generation Advanced Materials project, with support from Advantage West Midlands (AWM) and part funded by the European Regional Development Fund (ERDF). We thank the EPSRC and the University of Warwick for financial support. We thank the EPSRC National Crystallography Service (University of Southampton, UK) for data collection.

Notes and references

1 A. Werner and A. Vilmos, *Z. Anorg. Allg. Chem.*, 1899, **21**, 145–158.
2 C. R. Rice, *Coord. Chem. Rev.*, 2006, **250**, 3190–3199.
3 P. A. Gale and R. Quesada, *Coord. Chem. Rev.*, 2006, **250**, 3219–3244.
4 M. H. Keefe, K. D. Benkstein and J. T. Hupp, *Coord. Chem. Rev.*, 2000, **205**, 201–228.
5 V. Balzani, A. Juris, M. Venturi, S. Campagna and S. Serroni, *Chem. Rev.*, 1996, **96**, 759–834.
6 F. R. Keene, *Chem. Soc. Rev.*, 1998, **27**, 185–194.
7 F. R. Keene, *Coord. Chem. Rev.*, 1997, **166**, 121–159.
8 K. E. Erkkila, D. T. Odom and J. K. Barton, *Chem. Rev.*, 1999, **99**, 2777–2796.
9 C. Metcalfe and J. A. Thomas, *Chem. Soc. Rev.*, 2003, **32**, 215–224.
10 K. K.-W. Lo, K. H.-K. Tsang, K.-S. Sze, C.-K. Chung, T. K.-M. Lee, K. Y. Zhang, W.-K. Hui, C.-K. Li, J. S.-Y. Lau, D. C.-M. Ng and N. Zhu, *Coord. Chem. Rev.*, 2007, **251**, 2292–2310.
11 M. J. Clarke, *Coord. Chem. Rev.*, 2002, **232**, 69–93.
12 F. P. Dwyer and E. C. Gyarfas, *J. Proc. R. Soc. N. S. W.*, 1949, **83**, 174–176.
13 X. Hua and A. von Zelewsky, *Inorg. Chem.*, 1995, **34**, 5791–5797.
14 C. Hiort, P. Lincoln and B. Norden, *J. Am. Chem. Soc.*, 1993, **115**, 3448–3454.
15 S. Bodige, A. S. Torres, D. J. Maloney, D. Tate, G. R. Kinsel, A. K. Walker and F. M. MacDonnell, *J. Am. Chem. Soc.*, 1997, **119**, 10364–10369.
16 W. R. Browne, D. Hesek, J. F. Gallagher, C. M. O'Connor, J. S. Killeen, F. Aoki, H. Ishida, Y. Inoue, C. Villani and J. G. Vos, *Dalton Trans.*, 2003, 2597–2602.
17 J. Lacour, S. Torche-Haldimann, J. J. Jodry, C. Ginglinger and F. Favarger, *Chem. Commun.*, 1998, 1733–1734.
18 N. C. Fletcher, P. C. Junk, D. A. Reitsma and F. Richard Keene, *J. Chem. Soc., Dalton Trans.*, 1998, 133–138.
19 J. G. Collins, J. R. Aldrich-Wright, I. D. Greguric and P. A. Pellegrini, *Inorg. Chem.*, 1999, **38**, 5502–5509.
20 S. Torelli, S. Delahaye, A. Hauser, G. Bernardinelli and C. Piguet, *Chem.–Eur. J.*, 2004, **10**, 3503–3516.
21 N. C. Fletcher, M. Nieuwenhuyzen and S. Rainey, *J. Chem. Soc., Dalton Trans.*, 2001, 2641–2648.
22 A. Grabulosa, M. Beley and P. C. Gros, *Eur. J. Inorg. Chem.*, 2008, 1747–1751.
23 N. C. A. Baker, N. McGaughey, N. C. Fletcher, A. V. Chernikov, P. N. Horton and M. B. Hursthouse, *Dalton Trans.*, 2009, 965–972.
24 E. Meggers, *Chem.–Eur. J.*, 2010, **16**, 752–758.

25 L. Gong, S. P. Mulcahy, K. Harms and E. Meggers, *J. Am. Chem. Soc.*, 2009, **131**, 9602–9603.
26 P. Hayoz, A. Von Zelewsky and H. Stoeckli-Evans, *J. Am. Chem. Soc.*, 1993, **115**, 5111–5114.
27 A. von Zelewsky and O. Mamula, *J. Chem. Soc., Dalton Trans.*, 2000, 219–231.
28 N. C. Fletcher, C. Martin and H. J. Abraham, *New J. Chem.*, 2007, **31**, 1407–1411.
29 N. C. Fletcher, M. Nieuwenhuyzen, R. Prabarahan and A. Wilson, *Chem. Commun.*, 2002, 1188–1189.
30 H. Weizman, J. Libman and A. Shanzer, *J. Am. Chem. Soc.*, 1998, **120**, 2188–2189.
31 S. E. Howson, L. E. N. Allan, N. P. Chmel, G. J. Clarkson, R. van Gorkum and P. Scott, *Chem. Commun.*, 2009, 1727–1729.
32 C. P. Sebli, S. E. Howson, G. J. Clarkson and P. Scott, *Dalton Trans.*, 2010, **39**, 4447–4454.
33 S. E. Howson and P. Scott, *Dalton Trans.*, 2011, **40**, 4332–4333.
34 Y. Hsiao and L. S. Hegedus, *J. Org. Chem.*, 1997, **62**, 3586–3591.
35 D. A. Evans, G. S. Peterson, J. S. Johnson, D. M. Barnes, K. R. Campos and K. A. Woerpel, *J. Org. Chem.*, 1998, **63**, 4541–4544.
36 K. Sutowardoyo, M. Emziane and D. Sinou, *Tetrahedron Lett.*, 1989, **30**, 4673–4676.
37 R. N. Bream, S. V. Ley, B. McDermott and P. A. Procopiou, *J. Chem. Soc., Perkin Trans. 1*, 2002, 2237–2242.
38 Z. Y. Chang and R. M. Coates, *J. Org. Chem.*, 1990, **55**, 3475–3483.
39 F. J. LaRonde and M. A. Brook, *Inorg. Chim. Acta*, 1999, **296**, 208–221.
40 M. C. Thompson and D. H. Busch, *J. Am. Chem. Soc.*, 1962, **84**, 1762–1763.
41 S. Alshehri, J. Burgess, J. Fawcett, D. R. Russell and A. M. Shaker, *Transition Met. Chem.*, 2000, **25**, 691–694.
42 I. J. Munslow, A. J. Clarke, R. J. Deeth, I. Westmoreland and P. Scott, *Chem. Commun.*, 2002, 1868–1869.
43 P. D. Knight and P. Scott, *Coord. Chem. Rev.*, 2003, **242**, 125–143.
44 E. J. Crust, A. J. Clarke, R. J. Deeth, C. Morton and P. Scott, *Dalton Trans.*, 2004, 4050–4058.
45 I. J. Munslow, A. R. Wade, R. J. Deeth and P. Scott, *Chem. Commun.*, 2004, 2596–2597.
46 I. Westmoreland, I. J. Munslow, A. J. Clarke, G. Clarkson and P. Scott, *Organometallics*, 2004, **23**, 5066–5074.
47 I. Westmoreland, I. J. Munslow, A. J. Clarke, G. Clarkson, R. J. Deeth and P. Scott, *J. Organomet. Chem.*, 2006, **691**, 2228–2236.
48 A. G. Orpen, L. Brammer, F. H. Allen, O. Kennard, D. G. Watson and R. Taylor, *J. Chem. Soc., Dalton Trans.*, 1989, S1–S83.
49 F. A. Cotton and G. Wilkinson, *Advanced Inorganic Chemistry*, John Wiley & Sons, Inc., New York, 1988.
50 F. Tuna, M. R. Lees, G. J. Clarkson and M. J. Hannon, *Chem.–Eur. J.*, 2004, **10**, 5737–5750.
51 D. Pelleteret, R. Clerac, C. Mathoniere, E. Harte, W. Schmitt and P. E. Kruger, *Chem. Commun.*, 2009, 221–223.
52 J. A. Cowan, *Inorganic Biochemistry: An Introduction*, Wiley-VCH, New York, 1997.
53 P. Gütlich, Y. Garcia and H. A. Goodwin, *Chem. Soc. Rev.*, 2000, **29**, 419–427.
54 R. J. Dosser, W. J. Eilbeck, A. E. Underhill, P. R. Edwards and C. E. Johnson, *J. Chem. Soc. A*, 1969, 810–816.
55 B. J. Childs, D. C. Craig, M. L. Scudder and H. A. Goodwin, *Inorg. Chim. Acta*, 1998, **274**, 32–41.
56 R. Boca, P. Baran, L. Dlhán, J. Sima, G. Wiesinger, F. Renz, U. El-Ayaan and W. Linert, *Polyhedron*, 1997, **16**, 47–55.
57 M. J. Plater, P. Barnes, L. K. McDonald, S. Wallace, N. Archer, T. Gelbrich, P. N. Horton and M. B. Hursthouse, *Org. Biomol. Chem.*, 2009, **7**, 1633–1641.
58 A. Escuer, T. Comas, R. Vicente and J. Ribas, *Transition Met. Chem.*, 1993, **18**, 42–44.
59 A. Rodger and B. Nordén, *Circular Dichroism and Linear Dichroism*, Oxford University Press, Oxford, 1997.
60 M. Ziegler and A. von Zelewsky, *Coord. Chem. Rev.*, 1998, **177**, 257–300.
61 J. Hidaka and B. E. Douglas, *Inorg. Chem.*, 1964, **3**, 1180–1184.
62 E. G. Hohenstein and C. D. Sherrill, *J. Phys. Chem. A*, 2009, **113**, 878–886.
63 S. Grimme, *Angew. Chem., Int. Ed.*, 2008, **47**, 3430–3434.
64 E. J. B. A. Baerends, C. Bo, P. M. Boerrigter, L. Cavallo, L. Deng, R. M. Dickson, D. E. Ellis, L. Fan, T. H. Fischer, C. Fonseca Guerra, S. J. A. van Gisbergen, J. A. Groeneveld, O. V. Gritsenko, F. E. Harris, P. van den Hoek, H. Jacobsen, G. van Kessel, F. Kootstra, E. van Lenthe, V. P. Osinga, P. H. T. Philipsen, D. Post, C. C. Pye, W. Ravenek, P. Ros, P. R. T. Schipper, G. Schreckenbach, J. G. Snijders, M. Sola, D. Swerhone, G. te Velde, P. Vernooijs, L. Versluis, O. Visser, E. van Wezenbeek, G. Wiesenekker, S. K. Wolff, T. K. Woo and T. Ziegler, *adf2008.01*, Scientific Computing and Modelling NV: Free University, Amsterdam, 2008.
65 M. A. Robinson and D. H. Busch, *Inorg. Chem.*, 1963, **2**, 1171–1177.
66 A. Damianoglou, E. J. Crust, M. R. Hicks, S. E. Howson, A. E. Knight, J. Ravi, P. Scott and A. Rodger, *Chirality*, 2008, **20**, 1029–1038.
67 G. M. Sheldrick, *Acta Crystallogr., Sect. A: Found. Crystallogr.*, 1990, **46**, 467–473.
68 G. M. Sheldrick, *Acta Crystallogr., Sect. A: Found. Crystallogr.*, 2008, **64**, 112–122.
69 G. A. Bain and J. F. Berry, *J. Chem. Educ.*, 2008, **85**, 532–536.
70 S. Grimme, *J. Comput. Chem.*, 2004, **25**, 1463–1473.
71 E. J. Baerends, D. E. Ellis and P. Ros, *Theor. Chim. Acta*, 1972, **27**, 339–354.
72 C. C. Pye and T. Ziegler, *Theor. Chem. Acc.*, 1999, **101**, 396–408.
73 J. M. Janey, T. Iwama, S. A. Kozmin and V. H. Rawal, *J. Org. Chem.*, 2000, **65**, 9059–9068.
74 R. E. Cowley, R. P. Bontchev, E. N. Duesler and J. M. Smith, *Inorg. Chem.*, 2006, **45**, 9771–9779.
75 C. D. Bedford, R. N. Harris, R. A. Howd, D. A. Goff, G. A. Koolpe, M. Petesch, I. Koplovitz, W. E. Sultan and H. A. Musallam, *J. Med. Chem.*, 1989, **32**, 504–516.